# Performance of Millimeter Wave Massive MIMO with the Alamouti Code

# Performance du MIMO massif avec onde millimétrique et code d'Alamouti

A Thesis Submitted

to the Division of Graduate Studies of the Royal Military College of Canada

by

Alouzi Mohamed

In Partial Fulfillment of the Requirements for the Degree of

Master of Applied Science in Electrical Engineering

19 April, 2017

To my patient wife, helpful parents and loving children

# Abstract

Alouzi, Mohamed. M.A.Sc. Royal Military College of Canada, 19 April, 2017. Performance of Millimeter Wave Massive MIMO with the Alamouti code. Supervised by Dr. Francois Chan.

Severe attenuation in multipath wireless environments makes the performance of communication systems unreliable. Therefore, MIMO (multiple input multiple output) was proposed to provide a wireless system with diversity and spatial multiplexing. Massive MIMO was recently proposed to gain the advantage of conventional MIMO but on a much greater scale. Massive MIMO can achieve a much higher capacity without requiring more wireless spectrum; however, it is still difficult to implement because of some challenges, such as pilot contamination.

The need for higher data rate led researchers to propose another technique called Millimeter Wave (mmW) massive MIMO that offers a larger bandwidth compared to the current wireless systems. Because of the higher path loss at mmW frequencies, and the poor scattering nature of the mmW channel, directional beamforming techniques with large antenna arrays and the Alamouti coding scheme are used to improve the performance of the mmW massive MIMO systems. Computer simulations have shown that a gain of 15 dB or more can be achieved using the Alamouti code.

# Résumé

Alouzi, Mohamed. M.A.Sc. Collège militaire royal du Canada, 19 April, 2017. Performance du MIMO massif avec onde millimétrique et code d'Alamouti. Supervisé par le Dr Francois Chan.

L'atténuation sévère dans les environnements sans fil multi-chemins rend la performance des systèmes de communications non-fiable. Par conséquent, MIMO (en anglais, « Multiple-Input Multiple-Output » ou Entrée-Multiple Sortie-Multiple) a été proposé pour offrir de la diversité et multiplexage spatial à un système sans fil. Le MIMO massif a récemment été proposé pour obtenir l'avantage du MIMO conventionnel mais sur une échelle beaucoup plus grande. Le MIMO massif peut procurer une capacité beaucoup plus élevée sans nécessiter un spectre sans fil plus grand ; cependant, c'est encore difficile d'implémenter cette technique à cause de certains défis, comme la contamination du pilote.

Le besoin pour un taux de transmission plus élevé a conduit les chercheurs à proposer une autre technique, appelée MIMO massif avec onde millimétrique, qui offre une largeur de bande plus grande comparée aux systèmes sans fil actuels. A cause de la perte du chemin plus grande dans les fréquences millimétriques et de la dispersion plus faible du canal millimétrique, les techniques de formation de faisceau directionnel avec de grands réseaux d'antennes et le codage d'Alamouti sont utilisées pour améliorer la performance des systèmes MIMO massif avec onde millimétrique. Des simulations sur ordinateur ont montré qu'un gain de 15 dB ou plus peut être obtenu avec le code d'Alamouti.

Table of Contents

# List of Figures

# List of Algorithms

# List of Abbreviations

**ADC** analog to digital converter

**AOA** angle of arrival

**AOD** angle of departure

**AWGN** additive white Gaussian noise

**BPSK** binary phase shift keying

**BS** base station

**CS** compressed sensing

**CI models** close-in free space reference distance models

**CSI** channel state information

**DAC** digital to analog converter

**dB** decibels

**FDD** frequency division duplex

**LLSE** linear least squares estimator

**LOS** Line of sight

**MIMO** Multiple-Input Multiple-Output

**ML** maximum likelihood

**MMSE** minimum mean-squared error

**mmW** millimeter wave bands

**mmW massive MIMO** millimeter wave massive Multiple-Input Multiple-Output

**MRC** maximum ration combining

**MRT** maximum ratio transmission

**MS** mobile station

**NLOS** non-line of sight

**OFDM** orthogonal Frequency division multiplexing

**PLE** path loss exponent

**QPSK** quadrature symbol phase shift keying

**RF chains** Radio-Frequency chains

**SISO** Single-Input Single-Output

**SNR** signal-to-noise-ratio

**STBC** space-time block code

**STC** space-time code

**STTC** space-time trellis code

**SV model** Saleh Valenzuela model

**SVD** singular value decomposition

**TDD** time-division duplex

**ULAs** uniform linear arrays

**VBLAST** Vertical Bell Laboratories layered space-time

**ZF** zero-forcing

# List of Symbols

$\alpha$ - Normalization constant chosen to satisfy the power constraint

$\alpha_l$ - Complex gain of the $l^{th}$ path of mmW channel

$\theta_l$ - Azimuth angle of arrival

$\emptyset_l$ - Azimuth angle of departure

$a_{MS}(\theta_l)$ - Antenna array response vectors at the MS

$a_{BS}^{H}(\emptyset_l)$ - Antenna array response vectors at the BS

$\lambda$ - Wavelength of the mmW signal

$\sigma^2$- Variance of the noise

$\Psi$ - sensing matrix

$\mathcal{A}$ - Set of possible RF precoders based on phase shifters or a network of switches

$A_D$ - Dictionary matrix that consists of the antenna array response vectors at the MS and BS

$W_{RF}$ - Analog combiner

$W_{BB}$ - Baseband (digital) combiner

$W$ - Hybrid combiner

$W_{opt}$ - Unconstrained optimum digital combiner

$\mathcal{W}$ - MS training combining codebook

$W$- Massive MIMO linear detection matrix

$C$- STBC codeword

$\mathbf{C}$ - Capacity of MIMO Channels

$d_k$ - Complex large-scale fading coefficients

$f_d$ - Doppler Shift

$FSPL(f, 1\ m)$ - Free space path loss in dB at separation distance of 1m

$F_{BB}$ - Baseband (digital) precoder

$F$ - Hybrid precoder

$F_{opt}$ - Unconstrained optimum digital precoder

$F_{RF}$ - Analog precoder

$\mathcal{F}$ - BS training precoding codebook

$\frac{E_b}{N_0}$ – Signal-to-noise ratio relative to each uncoded information bit

$G_t$ - Transmitter antenna gains measured in dBi

$G_r$ - Receiver antenna gains measured in dBi

$g_{k,n}$ - Complex small-scale fading coefficients

$H$- MIMO channel matrix

$L$ - Number of paths at mmW channel

$L_d$ - Number of the dominant paths at mmW channel

$n$ - Complex Gaussian variable used to represent the AWGN

$N_t$ - Number of transmit antennas

$N_r$ - Number of receive antennas

$N_{BS}$ - Number of base station antennas

$N_{MS}$ - Number of mobile station antennas

$N_{RF}$ - Number of RF chains

$N_s$ - Number of data streams

$P_u$ - Uplink transmission power

$P_d$ - Downlink transmission power

$PL^{CI}(f, d)$ - Close-in (CI) free space reference distance path loss model at frequency $f$ and separation distance $d$

$P_r$ - Received power $P_r$ measured in dBm

$P_t$ - Transmit power$P_r$ measured in dBm

$\overline{P_R}$ - Average power gain

$R$ - Maximum achievable sum-rate or the spectral efficiency

$SINR_k$ - received signal-to-interference-plus-noise ratio (SINR) of the $kth$ user

$T^{BS}$ - Matrix where the contribution of the previously detected paths stored at the BS

$T^{MS}$ - Matrix where the contribution of the previously detected paths stored at the MS

$T_c$ - Time coherent of the fading channel

$X_\sigma^{CI}$ - The shadow fading standard deviation describing large-scale fluctuation about the mean path loss over distance and it is modeled by the log-normal distribution with 0 dB mean and standard deviation $\sigma$ measured in dB

Chapter 1

# Introduction

## 1.1 MIMO (Multiple-Input Multiple-Output) Evolution

Wireless networks have continued to develop and their uses have significantly grown. Cellular phones are nowadays part of huge wireless network systems and people use mobile phones on a daily basis in order to communicate with each other and exchange information.

MIMO (Multiple-Input Multiple-Output) is a wireless technique that utilizes an array of antennas to transmit a signal over a given frequency band, and at the receiving end an array of antennas to receive the signal. There are two techniques in MIMO to transmit data across a given channel that consists of different propagation paths [3]. The first technique, called spatial diversity or simply diversity, improves the reliability of the system by sending the same data across different propagation paths. The second technique increases the data rate of the system by transmitting different portions of the data stream on different propagation paths. This is called spatial multiplexing and it provides a multiplexing gain or degree of freedom.

In a MIMO system with a rich scattering environment, space-time codes (STC) and Vertical Bell Laboratories Layered Space-Time Architecture (V-BLAST) are designed to exploit the diversity and multiplexing gains, respectively with the knowledge of channel state information at either the receiver or transmitter [3]. A high data rate can be achieved by increasing the number of transmit antennas without increasing the transmission power and the use of spectrum. The motivation behind increasing the data rate or user capacity of a cellular system is to meet the demand for high data traffic in the upcoming years.

Massive MIMO [6], [16] has been proposed for 5G networks to achieve high capacity performance by using a very large number of transmit and/or receive antennas with transmit precoding and receive combining. In addition, significant improvement in communications quality of service (QOS), energy efficiency and in the reduction of the cost is expected in Massive MIMO. The simple linear precoding schemes, such as zero forcing precoding (ZF), Maximum-Ratio Transmission (MRT) and Minimum Mean-Square Error (MMSE) can be successfully implemented in massive MIMO. The same linear schemes can be used in the receive side. The data transmission is done by following the Uplink or Downlink scenarios. In the downlink, the Base Station (BS) uses the precoding matrices to precode the data symbols to a Mobile Station (MS) in the case of a single-user transmission or to several MSs for multi-user transmission. In the uplink the users send the data to the BS in their own cell where the data can be recovered by using linear processing techniques.

Although Massive MIMO is considered a good technique to achieve a high capacity, the channel estimation has to be performed in practice, similarly to the classical MIMO [6]. One way to estimate the channel state information in Massive MIMO is to use orthogonal pilot sequences. However, pilot contamination, where different users in different cells use the same orthogonal pilots because of the limited spectrum available, is one of the challenging problems that needs to be solved.

Another solution to increase the data rate is Millimeter Wave (mm Wave) cellular systems [7] [19]. Mm wave systems are able to transmit gigabits per second by taking advantage of the large bandwidth available at mm wave frequencies. Mm wave communications is a promising technology for future outdoor cellular systems. The path loss at mm wave frequencies makes it difficult to implement these systems [20], however because large antenna arrays can be packed

into small chips at mm wave frequencies, they provide a sufficiently powerful received signal [23]. Moreover, large antenna arrays help the design of beamforming techniques to direct the signal in a certain direction, hence reducing the path loss problem [20], [21], [22]. By using a baseband (digital) beamforming architecture, a high gain can be achieved, enabling multi-stream multi-users communications. However, large arrays of antennas make the baseband beamforming impractical because of the huge number of antennas, each requiring a power hungry RF chain. As a result, a digital beamforming architecture is difficult to implement as it leads to high power consumption and an increase of hardware complexity. Moreover, implementing baseband beamforming is based on the knowledge of the complete channel state information. Another beamforming design is Radio-Frequency (RF) beamforming, where both the precoder and combiner are done in the RF stage. Compared to digital beamforming, there are implementation advantages in terms of lower power consumption and lower hardware complexity because of the significantly reduced number of RF chains. Analog beamforming controls the phase of the transmitted signal at each antenna element via a network of analog phase shifters and is implemented in the RF domain. However, analog beamforming is subject to additional constraints, for example the phase shifters might be digitally controlled and have only quantized phase values. These constraints limit the potential of analog only beamforming solutions compared to digital beamforming.

A lot of research has been done to overcome the constraints required by analog beamforming. Several authors have proposed a hybrid beamforming structure that combines the strengths of both analog and digital beamforming systems to reduce hardware complexity [20][21][22]. The precoding and combining hybrid structure is done in both the baseband (BB) and RF sections. The performance of hybrid beamforming is close to the optimal digital one, which is practically

infeasible and has full-complexity, while the number of RF chains is reduced, i.e., $N_{RF} < N_T$ , where $N_{RF}$ is the number of RF chains and $N_T$ is the number of transmit antennas, resulting in a saving in power consumption and reduction of the hardware complexity.

## 1.2 Aim

The aim of this study is to minimize the bit error rate (BER) performance of a mmW massive MIMO system by using linear detection schemes and space time coding.

## 1.3 Contributions

In order to get a realistic communication system, the channel state information has to be estimated before designing the precoding and combining matrices of hybrid beamforming that support the transmission of multiple data streams and overcome the RF hardware limitation. Therefore, we adopt in this research a low complexity channel estimation algorithm [22]. Simulation results of the error probability with this estimation technique have not been published before.

By making the number of RF chains low enough to reduce the power and the hardware complexity, especially at the MS in a cellular system scenario, the error performance of mm Wave massive MIMO system goes down. Therefore, we use space time coding (STC), Maximum Likelihood (ML) detection, and Minimum Mean-Squared Error (MMSE) detection in this research to improve the system performance with a very low number of RF chains and assuming perfect mmW channel state information at the MS. Thesis topics will be described in Chapter 2. To our knowledge, simulation results of the error probability of these detectors are not

available in the literature. Similarly, the Alamouti code has never been applied to mmW massive MIMO. Computer simulations show that it can improve the performance by more than 15 dB.

## 1.4 Thesis Organization

The following chapters of this thesis are organized as follows:

- Chapter 2 will provide some background on classical MIMO, diversity methods, fading classification, functions and implementation of classical MIMO systems, and the capacity of multi-antenna channels. The section on massive MIMO will describe massive MIMO, and examine the linear detection schemes and maximum achievable sum-rate. The section on millimeter wave massive MIMO systems will explore the characteristics of mmW channel, and examine the path loss model, mmW channel model and beamforming design, including the channel estimation by using hybrid beamforming.
- Chapter 3 will provide simulation results of the Alamouti code implemented in classical MIMO systems, and will examine the performance of linear detection schemes used for the uplink and downlink of a single-cell massive multi user MIMO systems in the lower frequency bands. The section on the downlink performance of a single-cell hybrid beamforming mmW massive MIMO system will show how the schemes that are used by classical MIMO and massive MIMO, such as the maximum –likelihood (ML) detection, minimum mean-square error (MMSE) detection, and the Alamouti code can be exploited by hybrid beamforming mmW massive MIMO system to improve the overall error performance.
- Chapter 4 will conclude the thesis and provide recommendations for further research.

Chapter 2

# Background

## 2.1 Classical MIMO

In wireless communication, a channel may be affected by fading which will impact the performance of the system. To mitigate this, it was proposed in the previous chapter to use the diversity technique, i.e., to provide the receiver with multiple versions of the same signal. The principle of diversity guarantees that the probability that multiple version of a given signal are affected by fading at the same time is considerably reduced [11]. Therefore, diversity helps to improve the performance and to reduce the error rate.

Several diversity methods can be applied and provide a number of advantages. These methods are described as follows [44].

1. Time diversity: Using time diversity, a message may be transmitted at different times by using a channel code.
2. Frequency diversity: This form of diversity uses different frequencies. It is applied by using different channels, or a technology such as Orthogonal Frequency Division Multiplexing (OFDM).
3. Spatial Diversity (Antenna Diversity): Spatial diversity is one of the most popular forms of diversity used in wireless communication systems. Multiple and spatially separated antennas are employed to transmit or receive uncorrelated signals. Antenna separation should be at least half of the carrier wavelength to ensure sufficiently uncorrelated signals at the receiver.

In the past, fading or multiple paths were considered as an interference; however, by using the MIMO technique, these multiple paths can be turned to our advantage. They can be used to improve the signal to noise ratio or to increase the data rate [10].

In fading channels, a wireless communication environment Line-of-Sight (LoS) radio propagation path will often not exist between the transmitter and receiver because of natural and man-made obstacles situated between the transmitter and receiver. As a result the signal propagates via reflection, diffraction and scattering [11].

In MIMO, the system typically consists of $N_t$ antennas at the transmitter and $N_r$ antennas at the receiver as shown in the following figure [12]

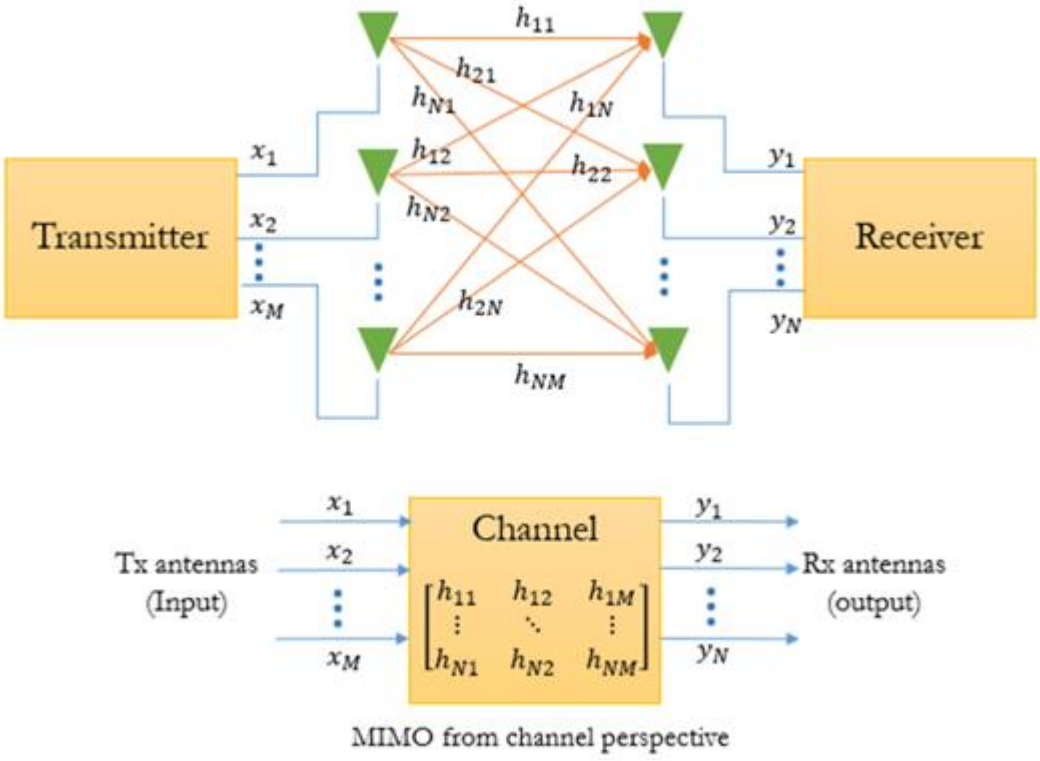


Figure 2.1. Multiple Input Multiple Output (MIMO) systems [12]

where each antenna not only receives the direct signal path (Line-of-Sight), but also a fraction of signal (Non- Line of Sight) due to the scattering, diffraction and reflection. The fading path between antenna 1 at the transmitter and antenna 1 at the receiver is represented by the channel response $h_{11}$. The channel response of the path formed between antenna 1 at the transmitter and antenna 2 at the receiver is expressed as $h_{21}$, and so on. Therefore, the dimension of the channel transmission matrix $H$ is $N_r \times N_t$, where $N_r$ is the number of receive antennas and $N_t$ is the number of transmit antennas.

The channel matrix is modeled by large-scale and small-scale fading [11]. The large-scale model or path loss model, which is caused by the path loss of the signal as a function of distance, and shadowing by large objects such as buildings and hills, is used to predict the received signal strength [11]. Small-scale fading, which is caused by the constructive and destructive interference of the multiple signal paths between the transmitter and receiver can be classified by four types [11]:

1. Slow fading: In slow fading, the channel matrix is quasi-static and the symbol period of the transmitted signal, $T_s$, is smaller than the channel coherence time, $T_c = \frac{0.423}{f_d}$ , where $f_d$ is the Doppler Shift. The channel coherence time is the time over which two symbols have a strong potential for amplitude correlation.
2. Fast fading: The symbol period of the transmitted signal is larger than the channel coherence time.
3. Flat fading: The bandwidth of the signal is smaller than the coherence bandwidth $B_c$ of the channel so the channel can be treated as flat.

4. Frequency selective fading: This occurs when the bandwidth of the signal is larger than the coherence bandwidth $B_c$ of the channel.

A flat fading signal, commonly assumed in wireless communication, follows the Rician distribution (LOS) or Rayleigh distribution (NLOS) [11].

The received vector $y$ is expressed in terms of the channel transmission matrix $H$ as follows

$$y = Hx + n$$

where $x$ is the transmitted symbols vector, $n$ is the vector of receiver noise whose elements are considered as zero-mean additive white Gaussian noise (AWGN) with variance of $\sigma^2$, and $H$ is the fading channel.

There are two main functions for MIMO system [11]:

- Spatial diversity: The same information-bearing signals are transmitted or received from multiple antennas, thereby improving the reliability of the system. Spatial diversity always refers to transmit and receive diversity.
- Spatial multiplexing: In this form of MIMO, the multiple independent data streams are simultaneously transmitted by many transmit antennas to achieve a higher transmission speed and increase the data rate of the system.

There are many technologies in MIMO that implement these two functions. In the following sections, the three best known techniques are described.

### 2.1.1 Space Time Block Codes

A Space-Time Block Code (STBC) involves the transmission of many versions of the data, which helps to mitigate the fading problems. Because of the redundancy in the transmitted data, some versions may experience less fading at the receiver [13].

When using STBC, the data stream is encoded in blocks before the transmission. The symbols in row 1 are simultaneously sent by the multiple antennas in time slot 1, then the symbols in row 2 are sent in time slot 2, etc. STBC can be expressed by the following matrix [13]

$$\begin{bmatrix} S_{11} & S_{12} & \cdots & S_{1N_t} \\ \vdots & & \ddots & \vdots \\ S_{m1} & S_{m2} & \cdots & S_{mN_t} \end{bmatrix}$$

where each row represents a time slot and each column represents different antennas. $S_{ij}$ is the modulated symbol to be transmitted in time slot $i$ from antenna $j$. There are $m$ time slots. Maximum Likelihood Decoding can be used at the receiver to detect the transmitted symbols. Next, we will talk about the most popular STBC, which is called the Alamouti Code.

#### 2.1.1.1 Alamouti Code

In this code, the number of transmit antennas $N_t$ is equal to two with any number of receive antennas $N_r$. For a given modulation scheme, if $s_1$ and $s_2$ are the selected symbols, the transmitter sends $s_1$ from antenna one and $s_2$ from antenna two in time slot one. Then, in time

slot two, it transmits $-s_2^*$ and $s_1^*$ from antennas one and two, respectively, where $s_i^*$ is the complex conjugate of $s_i$. Therefore, the transmitted codeword is [2] [3]

$$c = \begin{pmatrix} s_1 & s_2 \\ -s_2^* & s_1^* \end{pmatrix}$$

Let us assume that the channel is quasi-static with Rayleigh or Rician fading with unit variance and zero mean. Let the path gain from transmit antennas one and two to the receive antenna be $h_1$ and $h_2$. The decoder receives signals $r_1$ and $r_2$ in time slots one and two, respectively [2] [3].

$$r_1 = h_1 s_1 + h_2 s_2 + n_1$$

$$r_2 = -h_1 s_2^* + h_2 s_1^* + n_2$$

where $n_1$ and $n_2$ are Gaussian noise and independent from each other and the transmitted signals. For a coherent detection scheme where the receiver knows the channel gains $h_1$ and $h_2$, the combining scheme builds the following two signals [2] [3]:

$$\hat{s}_1 = h_1^* r_1 + h_2 r_2^*$$

$$\hat{s}_2 = h_2^* r_1 - h_1 r_2^*$$

where * is the complex conjugate. Then, the maximum–likelihood detection can then be used to detect the transmitted symbols by minimizing the decision metric as follows [2] [3]

$$s_1 = arg\min_{s_i} |s_i - h_1^* r_1 - h_2 r_2^*|^2$$

$$s_2 = arg\min_{s_j} \left|s_j - h_2^* r_1 + h_1 r_2^*\right|^2$$

The Alamouti code provides a full diversity code which is $N_t N_r = 2$, where $t = 2$ and $r$ is any number, and a full rate $R = 1$ because two symbols are detected in two time slots. It is proven that the performance of the Alamouti code with two transmit antenna is much better that that of the system with one transmit antenna, with more than 11dB improvement [2] [3]. However, all these desirable properties with the Alamouti code can only be achieved for two transmit antennas. Therefore, for a system with more than two transmit antennas, similar codes need to be designed; however, when the system has more than two transmit antennas, full rate cannot be achieved, except for generalized real orthogonal designs when $N_t \leq 8$ [3] [4]. This is one of the reasons why the Alamouti code is used in this thesis.

### 2.1.2 Space –Time Trellis Coding

Space-time trellis codes (STTCs) combine modulation and trellis coding to transmit information over MIMO channels. The symbols are transmitted simultaneously from different antennas and the Rayleigh or Rician fading wireless channel is quasi-static and frequency-nonselective. The goal of STTCs is to achieve maximum diversity, good performance, high data rate, and high coding gains [3] [14].

Data in STTCs are encoded and split into n streams that are simultaneously transmitted by using $N_t$ transmit antennas. The constructed codes provide a tradeoff between data rate, diversity advantage, and trellis complexity.

For simplification, consider two transmit antennas and one receive antenna. There are two symbols that are simultaneously transmitted from these two antennas for every branch in the trellis. For STTCs that send b bits/s Hz of information, $2^b$ branches leave each state. For example, as shown in the Figure 2.2 below [14], the code uses a QPSK (quadrature symbol phase shift keying) constellation, $b = 2$, with symbols $0,1,2,3$ to represent $1, j, -1, -j$, respectively [3] [14].

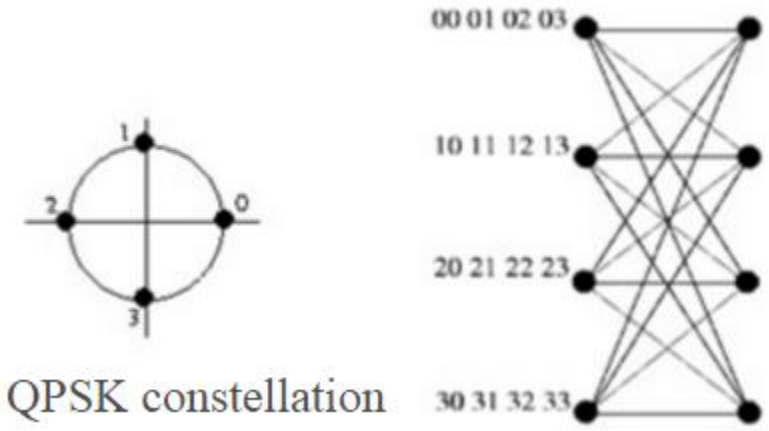


Figure 2.2. R=2 b/s/Hz, 4-PSK, 4-states, Diversity order is 2 [14]

The encoding starts at state zero which is represented by the first mod in Fig 2.2. Let's assume that the encoder is at state $S_t$ at time t, then b = 2 bits arrive at the encoder to pick one of the

$2^b = 4$ branches leaving state $S_t$. The two symbols $C_{t,1}$, $C_{t,2}$ of the selected branch are respectively sent from the two transmit antennas simultaneously. Then the encoder moves to state $S_{t+1}$. At the end of each frame, extra new bits are added to make sure that the encoder stops at state 0. Any valid codeword starts from state 0 and ends at state 0. A good design criterion that guarantees full diversity $N_t N_r$ is to make sure that for all possible codewords $C^i$ and $C^j$, $i \neq j$, the matrix $A(C^i, C^j)$ is full rank [3].

For the decoding of STTC, we assume that ideal channel state information is known to the decoder. The Viterbi algorithm can be used to decode STTCs and find the most likely path [14].

Although STTCs improves the reliability of the system, the decoding complexity increases with the number of states and with the number of transmit antennas [3] [14].

### 2.1.3 V- Blast Receiver

In the transmitter of V-Blast, the input bit stream is de-multiplexed into $N_t$ parallel substreams, where $N_t$ is the number of transmit antennas. Then each substream is modulated and transmitted from the corresponding transmit antenna. It is also possible to use coding for each substream to improve the performance in a trade-off with bandwidth. The decoding method in V-Blast employs successive interference cancellation (SIC), and the impact of each estimated symbol is canceled [15]. Flat fading is assumed and we consider the channel to be quasi-static over L symbol periods. Then, the corresponding received $y$-vector is [3] [15]

$$y = H \cdot x + n$$

where the vector $n$ is the vector of receiver noise whose elements are considered as zero-mean additive white Gaussian noise (AWGN), with variance of $\sigma^2$, $x$ is the transmit vector, and $H$ is the Rayleigh or Rician fading channels.

The detecting algorithm of V-Blast only works if the number of receive antennas is larger than or equal to the number of transmit antennas, $N_r \geq \mathrm{N}_t$. In this detecting algorithm, the receiver detects symbols one by one. After the first symbol is detected, the effects of this detected symbol in all the receive equation are canceled. Then, the second symbol is detected from the new sets of equation. The effects of the second detected symbol are also canceled to derive a new set of equations. This process continues until all symbols are detected [3] [15].

The detection algorithm includes three steps [3]:

1- Ordering

Certainly, the order in which the symbols are detected will impact the final solution. Therefore, the symbols with highest SNR (Signal-to-Noise ratio) are the first in the ordering step.

2- Interference nulling

There are many different methods to detect a symbol in the presence of interference. Some of these methods are minimum mean-squared error (MMSE) and Zero-Forcing nulling (ZF).

In the ZF method, in order to separately detect the symbols in the received vector y , we need to use the vector w that is called the Zero-Forcing nulling vector. The $N_r$ x 1 vector $w_{n_t}$ is orthogonal to the interference column vectors $\mathrm{h}_{n_t+1}$, $\mathrm{h}_{n_t+2}$,….. $\mathrm{h}_{N_t}$ but not orthogonal to column $\mathrm{h}_{\mathrm{n}_t}$. In other words, the vector w should be such that [3] [15]

$$\mathrm{h}_{n_t+1} \,.\, {w^T}_{n_t} = 0$$

$$\mathrm{h}_{\mathrm{n}_t} . {w^T}_{n_t} = 1$$

The vector w is calculated from the channel matrix H with dimension $N_r$ x $N_t$, with $N_r \geq N_t$. As a result of the multiplication, we get [3] [15]

$$y.\ {w^T}_{n_t} = x_{n_t} + n\ .\ {w^T}_{n_t}$$

where the noise is still Gaussian and the symbol $x_{n_t}$ can be decoded.

3- Interference Cancellation

The goal of the interference cancellation is to remove the already detected symbols in order to decode the next symbols [15]. Let's assume that the first symbol $x_1$ has been detected accurately, and then the first symbol's impact is canceled from received vector y by this equation [3]

$$y_1 = y - \hat{x_1}\ .\ h_1$$

where $\hat{x_1}$ is the first detected symbol. This step is repeated until all symbols are detected. Therefore, the VBLAST algorithm may eventually lead to significantly improved spectral efficiencies in wireless systems.

## 2.1.4 Capacity of Multi-Antenna Channels

MIMO technology offers very high capacity with increasing SNR for a large number of antennas at both transmitter and receiver. In the case of independent Rayleigh or Rician fading paths between antenna elements at both transmitter and receiver, the general capacity **C** expression is [45] [3]

$$\mathbf{C} = \log_2 \det\left(I_{N_R} + \left(\frac{SNR}{N_T}\right).\ H.H^H\right) \quad \text{bps/HZ}$$

where $N_R$ is the number of receive antennas, $N_T$ is the number of transmit antennas, small H stands for transpose conjugate, and $I_m$ is the m x m identity matrix.

In general, the capacity of a MIMO channel increases linearly with the number of antennas.

## 2. 2 Massive MIMO

In upcoming years, the amount of data traffic in wireless communication will increase considerably; therefore, a new generation network, 5G, has to be developed to increase the data capacity 1000 times compared to current 4G system [7]. Energy efficiency and faster communication response time are also expected in the future network [7]. In order to increase the spectral efficiency, you need to have one of the following options

1- Very large number of base station antennas [1] [16] [6] [17] [18].
2- Small cells [17].
3- In order to support more users, increasing the bandwidth by using the high frequency bands (millimeter Wave) is a very good choice.

In massive MIMO for example, the industry is trying to increase the number $N_t$ of BS antennas to 100 or more in order to simultaneously serve a large number of users $K$, say tens, with single or multiple antennas, in the same frequency band [1]. In addition, small cells are also expected in massive MIMO [7] [17]. The channel state information $H$ is the channel propagation matrix between the $K$ users and BS antennas array. In general, the channel propagation is modeled as a Rayleigh or Rician fading channel. In practice, the channel matrix has to be estimated by using orthogonal pilot sequences in the uplink transmission [7]. After estimating the channel state

information in the uplink transmission, the BS uses the estimated channel in downlink transmission to precode the data streams to all users.

Consider a Massive MU-MIMO BS with $N_t$ antennas that serves K single-antenna or multiple-antennas users. Denote the channel coefficient from the $k-th$ user to the $n-th$ antenna of the BS as $h_{k,n}$ in the uplink case, which is equal to a complex small-scale fading factor times an amplitude factor that accounts for geometric attenuation and large-scale fading[1] [8] [6]:

$$h_{k,n} = g_{k,n}\sqrt{d_k}$$

where $g_{k,n}$ and $d_k$ represent the complex small, and large-scale fading coefficients, respectively. The small-scale fading coefficients are assumed to be independent for each user, while the large-scale ones are the same for all the $N_t$ antennas but depend on the user's position [8]. Then, the channel matrix experienced by all the K users in the uplink scenario can be expressed as [8][6]

$$\begin{pmatrix} h_{1,1} & \cdots & h_{K,1} \\ \vdots & \ddots & \vdots \\ h_{1,N_t} & \cdots & h_{K,N_t} \end{pmatrix} = G\sqrt{D}$$

where

$$G = \begin{pmatrix} g_{1,1} & \cdots & g_{K,1} \\ \vdots & \ddots & \vdots \\ g_{1,N_t} & \cdots & g_{K,N_t} \end{pmatrix}$$

$$D = \begin{pmatrix} d_1 & \cdots & \dots \\ \vdots & \ddots & \vdots \\ \dots & \cdots & d_K \end{pmatrix}$$

In massive MIMO setup, as $N_t \gg K$, there are two system protocols, which are frequency-division duplex (FDD) or time-division duplex (TDD) used for data transmission [1]. The TDD scheme is more efficient than FDD because the channel estimation in TDD is reciprocal, which means that the estimated channel in the uplink case is the same as the downlink. Therefore, the estimated channel can be used by BS to precode the data streams. However, in FDD case, the channel estimation is not reciprocal [1][18].

The data transmission in massive MIMO as mentioned above is done by implementing the uplink or downlink techniques. Uplink transmission is the scenario where the $K$ users transmit signals to the BS. Let $S_k$ be the transmitted signal from the $kth$ user. Since the $K$ users share the same time-frequency resources, the $N_t$x1 received signal vector at the BS is modeled as follows [6][18][1]

$$y_u = \sqrt{P_u}\, HS + n_u$$

where $P_u$ is the uplink transmission power, $S \in C^{KX\,1}$ is the transmitted symbols from $K$ users, $n_u \in C^{N_t x 1}$ is the additive white noise vector with independent components, and $H \in C^{N_t X\, K}$ is the channel matrix.

With linear detection schemes at the BS, the transmitted symbols $\hat{S}$ can be detected by multiplying $y_u$ with the linear detection matrix $W \in C^{N_t\, X\, K}$ as follows [6][18]

$$\hat{S} = W^T y_u$$

Therefore, the received signal-to-interference-plus-noise ratio (SINR) of the $kth$ stream is given by [18]

$$SINR_k = \frac{P_u \left| w_k^{T^*} h_k \right|^2}{P_u \sum_{k \neq k'}^{k} \left| w_k^{T^*} h_{k'} \right|^2 + \|w_k\|^2}$$

where $w_k$ denotes the $kth$ column of matrix $W$.

Then, the maximum achievable sum-rate is given by [18]

$$R = \sum_{k=1}^{K} E\{log_2(1 + SINR_K)\}$$

where $E$ is the mean. The linear detection matrix $W$ can be designed by using one of the following techniques [18]

1- Maximum-Ratio Combining receiver (MRC):

We set $W$ equal to $H^*$, which is the complex conjugate of $H$. At low SNR, MRC can achieve the same array gain as in the case of a single-user system, but it performs poorly in multiuser interference.

2- Zero-Forcing Receiver:

By contrast to MRC, zero-forcing (ZF) receivers take the multiuser interference into account, but neglect the effect of noise. The ZF receiver matrix is the pseudo-inverse of the channel matrix H. With ZF, we have

$$W = H(H^H H)^{-1}$$

where the small $H$ is the transpose conjugate.

3- Minimum Mean-Square Error Receiver:

The linear minimum mean-square error (MMSE) receiver aims to minimize the mean-square error between the estimate $W'y_u$ and the transmitted signal$S$. Therefore, the MMSE receiver matrix is

$$W = H(H^H H + \sigma^2 I_K)^{-1}$$

where $I_K$ is the identity matrix, and $\sigma^2$ is the variance of the noise. MMSE receiver matrix works as MRC at low SNR and as ZF at high SNR.

In the downlink transmission scenario, the BS transmits data to all $K$ users. Let $X \in C^{Kx1}$ be the transmitted symbols vector intended for all $K$ users. Then by using linear precoding technique, the precoding vector $X_F$ [6] [19] is

$$X_F = \sqrt{\alpha} F X$$

where $F \in C^{N_t \, x \, K}$ is the precoding matrix, and $\alpha$ is a normalization constant chosen to satisfy the power constraint $E\{\|{X_F}^2\|\} = 1$ . Thus [18],

$$\alpha = \frac{1}{E\{tr(FF^H)\}}$$

Therefore, the received signal at $K$ users is given by [18]

$$y_d = \sqrt{P_d} H^T X_F + n_d$$

where $P_d$ is the downlink transmission power, $n_d \in C^{KX1}$ is a Gaussian noise vector, and $H^T \in C^{KxN_t}$ is the channel matrix.

By implementing the precoding techniques above, the $SINR_k$ is given as follows [18]

$$SINR_k = \frac{\alpha P_d \left| h_k{}^T f_k \right|^2}{\alpha P_d \sum_{k \neq k'}^{k} \left| h_k{}^T f_{k'} \right|^2 + 1}$$

where $f_k$ denotes the $k - th$ column of matrix $F$. Thus, the maximum achievable sum-rate in the downlink scenario is given by [18]

$$R = \sum_{k=1}^{K} E\{log_2(1 + SINR_K)\}$$

The three linear precoders are maximum-ratio transmission (MRT) (also called conjugate beamforming), ZF, and MMSE precoders; similarly, the precoding techniques have similar operational properties as MRC, ZF, and MMSE. The equations for these precoders are as follows [6][18]

$$F = \begin{Bmatrix} H, & \text{for MRT} \\ H(H^T H)^{-1}, & \text{for ZF} \\ H(H^T H + \frac{K}{P_d} I_K)^{-1}, & \text{for MMSE} \end{Bmatrix}$$

Although massive MIMO is promising for 5G networks, it has some drawbacks. As we know, the existing MIMO systems (such as LTE) are implemented with a small number of BS antennas $N_t$ (between 1 and 10) [7]. In this case, the number of RF (Radio-Frequency) chains, DACs (Digital-to-Analog converters), and ADCs (Analog-to-Digital converters), which are the most expensive and power-hungry parts of a wireless transceiver [7], can be the same as the number of BS antennas $N_t$. In addition, this small network has a light load, so a small number of active users is served at each time instant. Therefore, the problem of pilot contamination is not a big issue [7]. However, in a massive MIMO system with 100 or more BS antennas $N_t$, having $N_t$ RF chains is practically unfeasible because of the increasing cost and energy consumption. Specifically, when the transmission bandwidth is very large, the energy consumption of ADCs would be unacceptably high. Thus, there is ongoing research about utilizing hybrid beamforming, which uses a small number of RF chains, and using it in the channel estimation. In addition, in massive MIMO, a large number of active users is served at each time instant resulting in an increased number of orthogonal pilot sequences [7]. As a result, the system load becomes very high, and that causes the problem of pilot contamination, which is still an open research problem.

## 2.3 Millimeter Wave Massive MIMO Systems

Because massive MIMO has some drawbacks as we mentioned above, it is being considered in conjunction with millimeter wave (mmW) frequencies (i.e. carrier frequency $>$ 28 GHz), where many antennas can be packed into small chips. In addition, this new system offers a higher bandwidth (gigabits per second) and supports applications that require low latency by using mmW systems compared to the current communication system (4G) [19]. As a result, a mmW

massive MIMO system is able to meet the data rate demands in the upcoming years. It is particularly promising for future outdoor 5G systems [19].

The mmW frequency bands have different characteristics than the lower ones, so the new system needs different standards and modeling. For example, the mmW path loss is much higher than the low frequency's path loss, especially for NLOS paths [20]; however, using directional antennas can mitigate this higher path loss with 200m distance separation between the transmitter and receiver [23]. In addition, the need for directional antennas with mmW systems makes the delay spread, which is the difference between the time of arrival of the earliest significant multipath components and the time of arrival of the latest ones, much lower compared to low frequency bands [23]. Penetration losses also are much higher in indoor-to-outdoor scenarios, so the indoor users should not communicate with the outdoor base stations [20]. The advantage of packing many antennas in small chips and using directional antennas make the mmW channel model different [20][21]. MmW channels are often sparse in the angular and time domain [20][21][22], with a few scattering clusters and each of them with several rays ( a few paths exist including LOS path). Because of the smaller wavelength, a signal at mmW frequencies experiences the reflection and scattering in NLOS paths, but the diffraction is much lower. Therefore, mmW signals are attenuated by smaller objects such as human body, glass, trees and rain. The penetration loss caused by a human body is measured between 20 and 30 dB [20]. Finally, some properties that are true for low frequency systems such as multi-path delay spread, angle spread and Doppler shift are used again in mmW channel models [25].

### 2.3.1 Path Loss Model in Outdoor Scenario

As we mentioned above, the mmW antenna arrays have to be directional to overcome the higher path loss with 200m distance separation between the transmitter and receiver [23][26].

Therefore, it is critical to develop new models for system design. The large-scale propagation path loss at mmW is generated by different models; however, the close-in (CI) free space reference distance model is much popular, especially for outdoor environments [27][28]. The CI model is given as follows [27]:

$$PL^{CI}(f,d)[dB] = FSPL(f,1\,m)[dB] + 10nlog_{10}(d) + X_{\sigma}^{CI}$$

where $n$ denotes the path loss exponent (PLE) with reference distance 1m, $X_{\sigma}^{CI}$ is the shadow fading standard deviation describing large-scale fluctuation about the mean path loss over distance and it is modeled by the log-normal distribution with 0 dB mean and standard deviation $\sigma$ measured in dB, $d$ is the separation distance between the transmitter and receiver, and $FSPL(f,1\,m)$ denotes the free space path loss in dB at separation distance of 1m and is given by [27]

$$FSPL(f,1\,m)[dB] = 20log_{10}(\frac{4\pi f}{c})$$

where $c$ is the speed of light and $f$ is the carrier frequency. The separation distance between receiver and transmitter can range up to 200m in outdoor scenarios. For a larger distance (> 200 meter), the receiver signal strength becomes difficult to capture [26] [27].

The received power $P_r$ measured in dBm, given the transmit power $P_t$, can be expressed as follows [25]

$$P_r[dBm] = P_t[dBm] + G_t[dBi] + G_r[dBi] - PL^{CI}(f,d)[dB]$$

where $G_t$ and $G_r$ are the transmitter and receiver antenna gains in dBi, respectively.

### 2.3.2 Channel Model and Beamforming Design

Due to the small wavelength of signals at mmW frequency bands, it is mentioned above that large arrays can be used at both the transmitter and receiver to direct a beam in a certain direction in order to get the strongest received power [23]. Therefore, beamforming schemes can be exploited to mitigate the high path loss. As a result, the channel models are different for mmW massive MIMO systems [20].

#### A- Channel Model:

The limited spatial selectivity or scattering characteristic in outdoor scenarios of mmW massive MIMO channel caused by high path loss [20], can be captured by a common model called Saleh-Velenzuela (SV) model [21][31], where the narrow band channel matrix H can be modeled as follows [22]

$$H = \sqrt{N_{BS}N_{MS}} \sum_{l=1}^{L} \alpha_l a_{MS}(\theta_l) a_{BS}^H(\emptyset_l)$$

where $N_{BS}, N_{MS}$ are the number of BS and MS antennas respectively, $\alpha_l$ is the complex gain of the $l^{th}$ path and it is assumed to be Rayleigh distributed, i.e., $\alpha_l \sim \aleph(0,\overline{P_R})$ , $l = 0,1, \dots L$ with $\overline{P_R}$ the average power gain, and $\emptyset_l, \theta_l$ are the $l^{th}$ path's azimuth angles of departure and arrival (AODs/AOAs) of the BS and MS, respectively, with uniform distribution. $L$ is the number of paths in a cluster. In this research, we consider the azimuth angles only without adding elevation (2-D channel model), and that means that only 2-D beamforming is used. The 3-D beamforming

and 3-D channel models can also be used in mmW massive MIMO system, but most papers in the literature use the 2-D model [21]. Lastly, $a_{MS}(\theta_l)$ and $a_{BS}^{H}(\emptyset_l)$ are the antenna array response vectors at the MS and BS, respectively. They are applied by uniform linear arrays (ULAs), but they can be applied by different antennas arrays [21]. ULA is given by [21]

$$a_{BS}^{H}(\emptyset_l) = \frac{1}{\sqrt{N_{BS}}}[1, e^{j\left(\frac{2\pi}{\lambda}\right) d\, sin(\emptyset_l)}, \dots, e^{j(N_{BS}-1)\left(\frac{2\pi}{\lambda}\right) d\, sin(\emptyset_l)}]^T$$

where $\lambda$ is the wavelength of the mmW signal, and $d$ is the distance between the antenna elements, typically $d = \frac{\lambda}{2}$. The array response vectors for MS can also be done as above.

## B- Beamforming Designs:

The small wavelength of signals in the mmW frequency bands allows a large number of antenna elements (32 or more) to be packed in a small physical space [25][24]. In order to generate a beam, you need to control the phase of the signal that is transmitted or received by each antenna element to achieve a high antenna gain in certain direction and low gain in the other directions [24]. In addition, creating a beam between the transmitter and receiver can be done by obtaining the best received power signal or maximum data rate [20]. There are different beamforming designs in mmW MIMO systems as described below.

### 1- Digital Beamforming

Although digital beamforming is hard to implement in practice [25][32] as we will explain later, it shows its strength when it is combined with analog beamforming. In digital beamforming, all the signal processing is done at baseband [20][25][32], where each RF chain is connected to each antenna element, with $N_{RF} = N_t$ as shown in Figure 2.3 (a) [20]. In digital beamforming,

the transmitter can transmit a single data stream or multiple data streams $N_s$ to one receiver or spatially multiplexed into different receivers [32]. The precoding and combining matrices are optimum in digital beamforming which are created by using channel state information (CSI) $H$ [25], but digital beamforming is very sensitive to imperfect CSI [32]. On the other hand, there are hardware constraints that make digital beamforming unfeasible in practice [25][20]. These limitations, which are caused by large antenna elements, high carrier frequencies at mmW bands, and large signal bandwidth are summarized as follows [25] [20]

- An RF chain to each antenna of a mmW massive MIMO system increases the power consumption and the cost of the system.
- The very small separation between all antenna elements make it hard to use a complete RF chain for each antenna.

Because of these hardware constraints, Analog Beamforming design and Hybrid Beamforming design have been proposed to comply with these constraints.

## 2- Analog Beamforming

In analog beamforming, all the signal processing is done in the RF domain [25][20]. As shown in Figure 2.3 (b) [20], phase shifters are connected to each antenna element. In addition, all phase shifters are applied to a single RF chain to transmit a single data stream [32]. The phase shifter weights are controlled digitally to direct the beam to a certain direction based on the best received signal power and maximum data rate [25][32].

Let us consider the downlink scenario, where BS transmits a symbol $S$ to a user by using analog beamforming. In this case, we have only one analog beam $F_{RF}$ directed to the user. The best beam gives the best received signal power at the user. Then, the transmitted vector $y$ is given by [20]

$$y = F_{RF}\, S$$

where the analog precoder $F_{RF}$ is implemented by limited quantized phase shifters [20][32][25]. As a result, $F_{RF}$ is written as follows [20]

$$F_{RF} = \frac{1}{\sqrt{N_{BS}}}\left[1, e^{j\emptyset_1}, \ldots, e^{j\emptyset_{N_{BS}}}\right]$$

which is equal to the array response vector in the strongest direction [33] and $\emptyset_n, n = 1, \ldots . N_{BS}$ are designed to direct a beam in a certain direction maximizing the received signal power. Channel estimation can be exploited in analog beamforming by using beam training. Using a codebook of beam patterns with different resolutions is very common for mmW channel estimation [20][32].

Although analog beamforming meets the hardware constraint of mmW massive MIMO systems and is not sensitive to the imperfect mmW channel [32], it is limited by the quantized phase shifters controlled digitally [25][20]. In addition, based on the results in [32], analog beamforming's performance is not achievable at NLOS and LOS in the case of increasing the number of RF chains because of the problem of interference and phase shifter errors respectively. Therefore, an analog beamforming transmitter should support a single receiver with a single RF chain transmitting a single data stream. These drawbacks in analog beamforming have led to the need to design Hybrid beamforming.

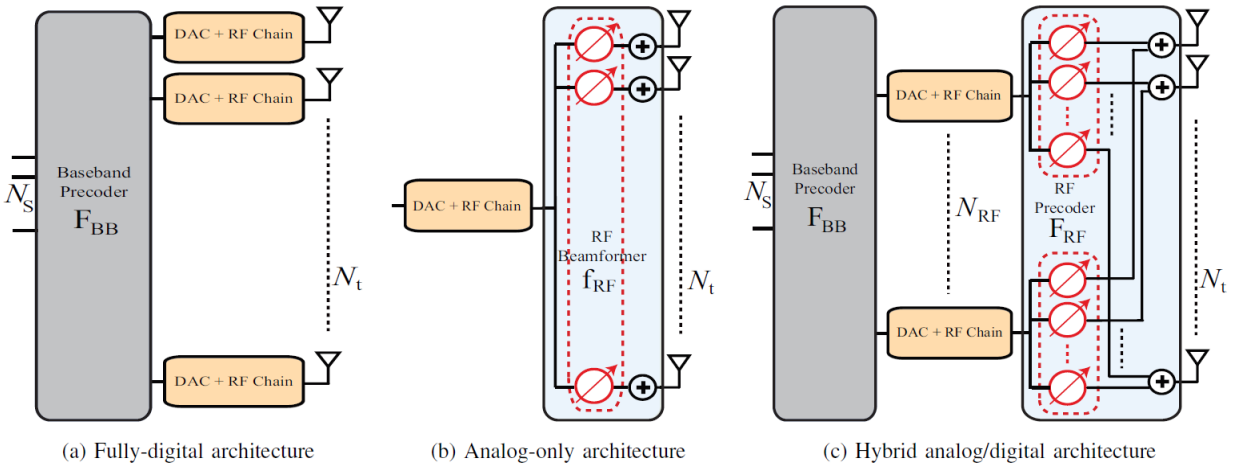


Figure 2.3. This figure shows a transmitter having $N_t$ antennas with a fully-digital, analog-only, or hybrid analog/digital architecture. In the hybrid architecture, $N_{RF} \ll N_t$ RF chains are deployed [20].

## 3- Hybrid Beamforming Solutions

Hybrid beamforming consists of both digital and analog beamforming design [20][25]. Therefore, because its architecture is implemented in the analog and digital domain, it offers a good performance with lower hardware complexity. In addition, its performance is close to the unconstrained digital beamforming [20]. As we see in Figure 2.3 (c) [20], the hybrid precoding is implemented in the digital and analog domain giving $F_{BB}$ (baseband precoder) and $F_{RF}$ (RF precoder) respectively. In hybrid precoding, the number of RF chains is larger than one and smaller than the number of transmitter antennas $N_t$. This allows the transmitter to communicate with one receiver by multiple data streams or communicate with multiple receivers by a single data stream where, $N_s \leq N_{RF} \ll N_t$ [20][25]. Therefore, hybrid beamforming achieves spatial multiplexing gains [20][25].

Consider two hybrid beamforming implemented by BS and MS with $N_{RF}$ RF chains

as shown in Figure 2.4 [22]. Assume BS with $N_{BS}$ antennas communicates with a single MS with $N_{MS}$ antennas. The BS and MS communicate using $N_s$ data streams with $N_s \leq N_{RF} \ll N_{BS}$ in the BS, and $N_s \leq N_{RF} \ll N_{MS}$ in the MS. Consider the downlink transmission. The BS applies an $N_{RF}$ x $N_s$ baseband precoder $F_{BB}$ followed by an $N_{BS}$ x $N_{RF}$ RF precoder $F_{RF}$. As a result, $N_{BS}$ x $N_s$ hybrid precoder $F$ is equal to $F_{RF}\, F_{BB}$. The hybrid combiner $W \in C^{N_{MS} \text{ x } N_s}$ is also equal to $W_{RF}\, W_{BB}$.

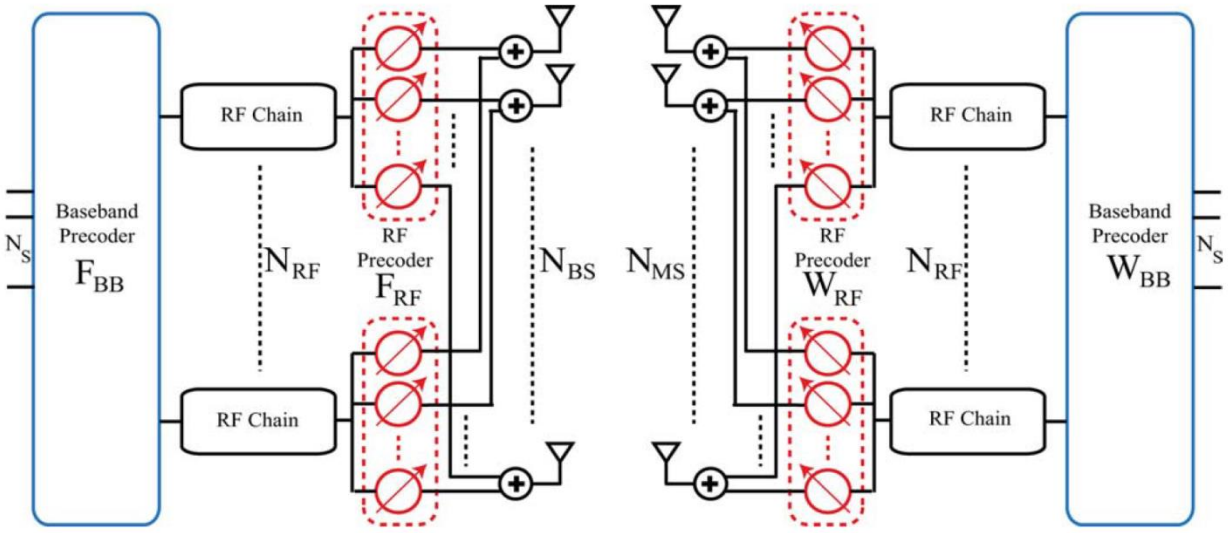


Figure 2.4. Block diagram of BS-MS transceiver that uses RF and baseband beam-former at both ends [22].

The RF precoder/combiner is implemented by phase shifters, so they are normalized to have the same amplitude with different phase only such that $|F_{RF}|^2 = \frac{1}{N_{BS}}$ and $|W_{RF}|^2 = \frac{1}{N_{MS}}$ [21][22]. In addition, the baseband precoder/combiner is normalized to satisfy the total power constraint such that $\|F_{RF}F_{BB}\|_F^2 = N_S$, and $\|W_{RF}W_{BB}\|_F^2 = N_S$ [21][22].

In this research, we consider a narrowband block-fading channel model. Then, the received signal $y$ is combined at the MS as follows [22]

$$y = W^H(\sqrt{P_r}HFS + n) \quad (2.1)$$

where $H$ is the $N_{MS}$ x $N_{BS}$ mmW channel matrix in the downlink transmission between BS and MS, $S \in C^{N_s \mathrm{x} 1}$ are the transmitted symbols, where $E[SS^H] = \frac{1}{N_s} I_{N_s}$, where $I_{N_s}$ is the $N_s$ $by$ $N_s$ identity matrix, $P_r$ is the average received power, and $n$ is a $N_{MS}$ x 1 Gaussian noise vector with zero mean and variance $\sigma^2$. Equation 2.1 is called the combined system in Chapter 3. The uplink transmission can be done in the same way, with $H \in C^{N_{BS} \mathrm{X} N_{MS}}$ and reversing the roles of the precoders and combiners.

As explained in Chapter 3, by assuming a perfect channel state information at the MS, we can use the effective channel at the MS given as follows [46]

$$H_{efe} = W^H HF$$

to detect the transmitted data streams using ML and MMSE detectors. In addition, the effective channel can be used by the Alamouti code to decode the transmitted data streams. Note that the dimension of these effective channels is much less than the original mmW channel matrix $H$. These effective channels can be generated by MS using the mmW channel.

Hybrid beamforming can achieve spatial multiplexing by transmitting multiple data streams [20][25]. In addition, it offers more degrees of freedom compared to the analog beamforming, where the beam can be steered in the azimuthal/vertical direction owning to its digital processing layer [20]. It can also correct the degradation caused by the $F_{RF}$ precoder/combiner in the case of interference by using the $F_{BB}$ precoder/combiner [25]. That is why the hybrid beamforming is preferred compared to analog and its performance is close to the unconstrained digital beamforming. In addition, [34][35] proposed a network of switches instead of phase shifters, and

the few bit-ADC (Analog to digital converter) technique, respectively to achieve low power consumption and low complexity.

Finally, the spectral efficiency achieved by hybrid beamforming is given by [25][22][21]

$$R = log_2 \left| I_{N_s} + \frac{P_r}{N_s} R_n^{-1} W_{BB}^H W_{RF}^H H F_{RF} F_{BB} F_{BB}^H F_{RF}^H H^H W_{RF} W_{BB} \right|$$

where $R_n = \sigma_n^2 W_{BB}^H W_{RF}^H W_{RF} W_{BB}$ is the post-processing noise covariance matrix in the downlink, and $R_n = \sigma_n^2 F_{BB}^H F_{RF}^H F_{RF} F_{BB}$ in the uplink.

In this research, we analyze a single data stream to a single user by using analog beamforming, and multiple data streams to single user hybrid precoders/combiners in a mmW massive MIMO system, as described in the next sections.

### 2.3.3 Single Data Stream and Single User by Using Analog Beamforming

When BS and MS use analog beamforming, they use the antenna array to communicate with each other by a single data stream. Assume $F_A$ and $W_A$ are the analog precoder and analog combiner respectively, then the receiver $SNR$ is given by [20]

$$SNR = \frac{|W_A^H H F_A|^2}{\sigma^2}$$

Therefore, the goal of analog precoders/combiners is to maximize this received $SNR$.

Because of the limited scattering characteristics in outdoor mmW channels, it becomes easier to direct a beam with higher gain in a strongest/desired direction $\emptyset_s$.

It is found that making the beamforming weights to match the array response vector in the desired direction is the best way to generate analog precoders/combiners [20]. That means, set $W_A = a_{MS}(\theta_s)$ and $F_A = a_{BS}(\emptyset_s)$ in the case of MS and BS respectively. The beampattern,

pointed to the desired direction, with main-lobe gain $G_{BS}$, and side-lobe gain $g_{BS}$ is shown in Figure 2.5 [20].

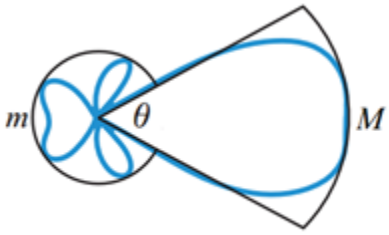


Figure 2.5. Approximated sectored-pattern antenna model with main-lobe gain $G_{BS}$, and side-lobe $g_{BS}$ [20].

### 2.3.4 Multiple Data Streams and Single User by Using Hybrid Design

Hybrid precoders are built in a way that maximizes the spectral efficiency $R$ [22][21]. In addition, the RF precoders constraint and baseband power constraint are taken into account. As we mentioned above, the mmW channels are expected to have limited scattering; therefore, hybrid precoders are built to approximate the unconstrained optimum digital precoder $F_{opt}$ to maximize the spectral efficiency of the system [21][22][25]. Most of hybrid precoders, $F_{opt}$ is given by the channel singular value decomposition (SVD) [36] such that

$$[U\ \Sigma\ V^H] = SVD(H)$$

By taking the largest $N_s$ of the system, then

$$F_{opt} = \ V \in C^{N_{BS}\,\mathrm{x}\,N_S}$$

$$W_{opt} = U \in C^{N_{MS} \times N_S}$$

Therefore, the hybrid precoder is found as follows [20][21][22]

$$(F_{RF}^*, F_{BB}^*) = argmin \left\| F_{opt} - F_{RF} F_{BB} \right\|_F$$

$$s.t. F_{RF} \in \mathcal{A}$$

$$\|F_{RF} F_{BB}\|_F^2 = N_S$$

and it can be solved by finding the projection of $F_{opt}$ on the set of hybrid precoders $F_{RF}F_{BB}$ with $F_{RF} \in \mathcal{A}$, where $\mathcal{A}$ is the set of possible RF precoders based on phase shifters or a network of switches. The hybrid combiners can be done in the same way.

Lastly, In order to achieve high spectral efficiency in mmW massive MIMO system by using hybrid precoders, the number of data streams $N_s$ should be close to the number of dominant channel paths in mmW [20].

### 2.3.5 Channel Estimation by Using Hybrid Beamforming

In order to estimate mmW channel, different parameters of each channel path $l$ need to be estimated. These parameters are AOAs (Azimuth Angles of Arrival), and AODs (Azimuth Angles of Departure) and the path gain of each path. In this research, we adopt the way of estimating the mmW channel that is used in [22]. Because of the poor scattering nature of the mmW channel, its estimation problem can be formulated as a sparse problem. By considering this type of solution, [22] has proposed algorithms that use multi-resolution codebook to estimate the mmW channel.

## (a) A Sparse Formulation of MmW Channel Estimation Problem

In this research, we consider the use of hybrid beamforming design and mmW channel model that we described in Section 2.3.2.

When the BS uses a beamforming vector $f$, then the MS combines the received signal by using the measurement vectors $W$, where $W = [W_1, W_2, \ldots . W_{M_{MS}}]$ is the $N_{MS}$ x $M_{\ MS}$, and $M_{\ MS}$ is the number of measurement vectors. If the BS use $M_{BS}$ beamforming vectors $F_P = [f_1, f_2, \ldots . f_{M_{BS}}]$, with $N_{BS}$ x $M_{BS}$, at different time slots and the MS use the same measurement matrix $W$ to combine the received signal, then the received vectors $Y = [y_1, y_2, \ldots . y_{M_{BS}}]$ can be processed as follows [22]

$$Y = W^H HFS + Q$$

where $Q$ is a $M_{MS}$ x $M_{BS}$ Gaussian noise matrix. The matrix $S = [s_1, s_2, \ldots s_{M_{BS}}]$ is the transmitted symbols. For the training phase, it is assumed that all the transmitted symbols are equal; therefore, $S = \sqrt{P}\, I_{M_{BS}}$, where $P$ is the average power vector used per transmission in the training phase. Then, the processed received vectors $Y$ can be rewritten as follows [22]

$$Y = \sqrt{P} W^H HF + Q$$

In order to use the sparse solution, the matrix $Y$ needs to be vectorized as follows [22]

$$y_v = \sqrt{P}\, VEC(W^H HF) + VEC(Q)$$

$$= \sqrt{P}\, (F^T \otimes W^H)(A_{BS}^* \text{ o } A_{MS}^*) + VEC(Q)$$

where $(F^T \otimes W^H)$ represents the Khatri-Rao product [37], and the matrix $(A_{BS}^* \circ A_{MS}^*)$ is an $N_{BS}N_{MS}$ x $L$ matrix in which each column has the form ( $a_{BS}^*(\emptyset_l) \otimes a_{MS}(\theta_l)$, $l = 1,2 \dots L$ where each column $l$ represents the Kronecker product of the BS and MS array response vectors for the AOA/AOD of the $l$th path of the channel [22].

It is assumed that AOAs/AODs are taken from a uniform grid of $N$ points [38][39][40], where $N \gg L$; therefore, $\emptyset_l, \theta_l \in \left\{0, \frac{2\pi}{N}, \dots . \frac{2\pi(N-1)}{N}\right\}$, where $l = 1,2, \dots L$. The $y_v$ can be approximated as follows [22]

$$y_v = \sqrt{P}\,(F^T \otimes W^H)A_D Z + VEC(Q)$$

where $A_D$ is a $N_{BS}N_{MS}$ x $N^2$ dictionary matrix that consists of the $N^2$ column vectors of the form ( $a_{BS}^*(\overline{\emptyset}_u) \otimes a_{MS}(\overline{\theta}_v)$, where $\overline{\emptyset}_u = \frac{2\pi u}{N}$ , $u = 0,1 \dots N-1$ and $\overline{\emptyset}_v = \frac{2\pi v}{N}$ , $v = 0,1 \dots N-1$. $Z$ is a $N^2$ x 1 vector that has the path gains of the channel paths.

The detection of the column $A_D$ that is associated with the non-zero elements of $Z$ means the detection of the AOAs and AODs of the dominant paths of the channel. Knowing that $Z$ has only $L$ non-zero elements, then the number of required measurements to detect these elements is much less than $N^2$.

If we define the sensing matrix $\Psi = (F^T \otimes W^H)A_D$ , then the goal of the compressed sensing algorithm is to design this sensing matrix to recover the non-zero elements of the vector $Z$ [41]. Note that $\Psi$ and $Z$ are incoherent.

In order to estimate the mmW channel, an adaptive compressed sensing solution that uses the training beamforming vectors is utilized.

## (b) Adaptive Compressed Sensing Solution

By assuming the use of hybrid beamforming, the process at adaptive CS is divided into a number of stages. The training precoding and the measurements are used at each stage and they are determined by the earlier stages. By using the training process which is divided into $S$ stages, the vectorized received signals are given as follows [42][43][22]

$$y_1 = \sqrt{P_1}\,({F_1}^T \otimes {W_1}^H) A_D Z + n_1$$

$$y_2 = \sqrt{P_2}\,({F_2}^T \otimes {W_2}^H) A_D Z + n_2$$

$$\vdots$$

$$y_S = \sqrt{P_S}\,({F_S}^T \otimes {W_S}^H) A_D Z + n_S$$

The design of $F$ and $W$ of each stage depends on $y_1, y_2, \ldots . y_{S-1}$ in the training process. The range of AOAs/AODs is divided at each stage into smaller ranges until the required resolution is achieved. That is corresponding to the division of the vector $Z$ into a number of partitions. The vectorized signals $Y$is used at each stage to determine the partitions that are more likely to have the non-zero elements. In the last stage of the training process, one path is detected and that is corresponding to the detection of AOA/AOD with the required resolution. By detecting these angles, the path gain of each path can be estimated.

The next section gives more information about the design of a multi-resolution beamforming codebook which is used by the adaptive CS solution to estimate the mmW channel.

### 2.3.6 Hybrid Precoding Based Multi-Resolution Hierarchical Codebook

In this sub-section, we provide some information about a multi-resolution beamforming vector codebook which is made by using a hybrid beamforming design. The design of the BS training precoding codebook $\mathcal{F}$ is similar to the MS one.

For simplification, we will focus in this research on the BS precoding codebook $\mathcal{F}$.

#### 2.3.6.1 The Design of the Codebook Beamforming Vectors

The BS precoding codebook consists of $S$ levels, with $\mathcal{F}_S$, $s = 1,2, \ldots . (S-1)$. Each level has beamforming vectors with a certain beamwidth (certain combination of the AOD angles) to be used in the channel estimation algorithm. The beamforming vectors at each codebook level $s$ are divided into $K^{S-1}$ subsets, with $K$ beamforming vectors at each subset. There is a unique range of the AODs at each subset $k$. In addition, these ranges are equal to $\left\{\frac{2\pi u}{N}\right\}_{u \in \mathrm{I}_{(s,k)}}$, where $\mathrm{I}_{(s,k)} = \left\{\frac{(k-1)N}{K^{S-1}}, \ldots\ldots, \frac{kN}{K^{S-1}}\right\}$, with $N$ the needed resolution parameter. The AOD range is further divided into $K$ sub-ranges, and each of the $K$ beamforming vectors is designed to have an almost equal projection on the array response vectors $a_{BS}(\overline{\emptyset}_u)$ and zero projection on the other vectors $a_{BS}(\overline{\emptyset}_{u \neq u})$.

The beamforming vector is designed for a certain beamwidth and is determined by these sub-ranges at each stage. Figure 2.6 shows the first three stages of codebook with $N = 256$ and $K = 2$ and Figure 2.7 depicts the beam patterns of each codebook level.

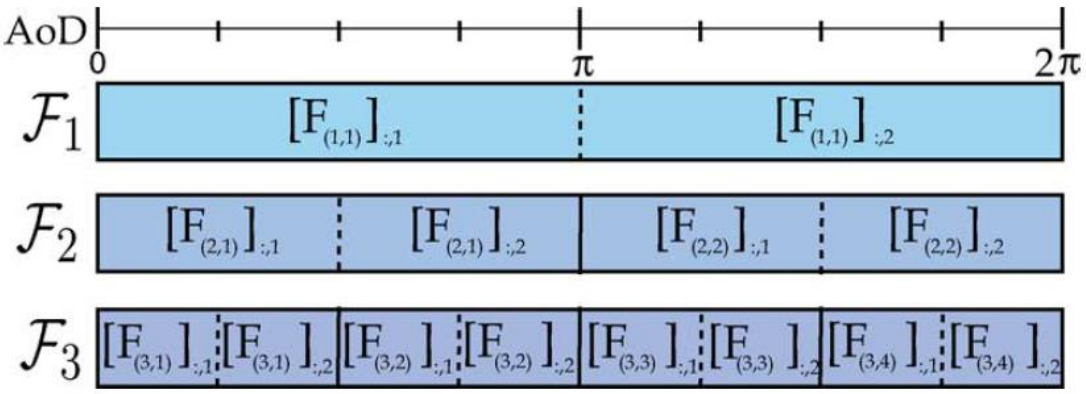


Figure 2.6. An example of the structure of a multi-resolution codebook with a resolution parameter $N = 256$ and $K = 2$ with beamforming vectors in each subset [22].

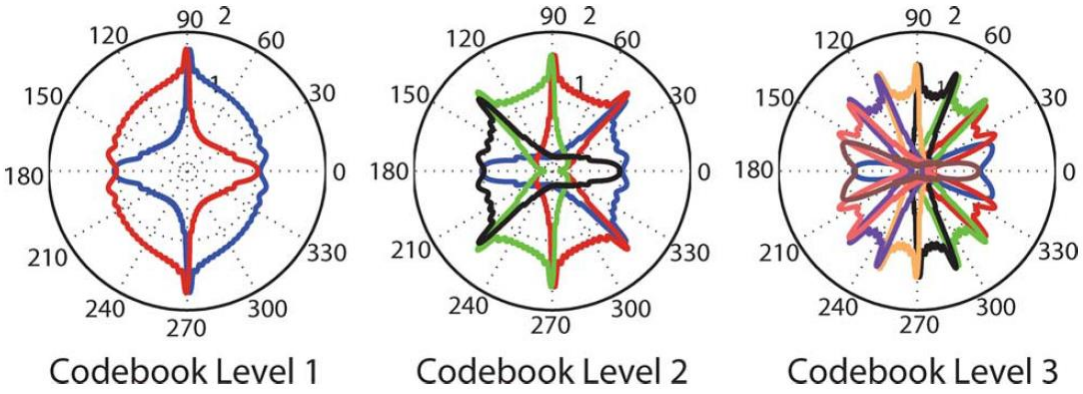


Figure 2.7. The resulting beam patterns of the beamforming vectors in the first three codebook levels [22].

Now let us look at the design of the codebook beamforming vectors used for mmW channel estimation. This design is proposed by [22]. In each codebook with level $s$, and subset $k$, the beamforming vectors $\left[F_{(s,k)}\right]_{:,m}$ $m = 1,2, \ldots . K$ are designed as follows

$$\left[F_{(s,k)}\right]_{:,m} a_{BS}(\overline{\emptyset}_u) = \begin{Bmatrix} C_s & if\ u \in \mathrm{I}_{(s,k,m)} \\ 0 & if\ u \notin \mathrm{I}_{(s,k,m)} \end{Bmatrix}$$

where

$$\mathrm{I}_{(s,k,m)} = \left\{ \frac{N}{K^s}(K(k-1)+m-1)+1, \ldots, \frac{N}{K^s}(K(k-1)+m) \right\}$$

is the sub-range of AODs associated with the beamforming vector $\left[F_{(s,k)}\right]_{:,m}$, and $C_s$ is a normalization constant that satisfies $\left\|F_{(s,k)}\right\|_F = K$. For example, the beamforming vector $\left[F_{(2,1)}\right]_{:,2}$ in Figure 2.6 is designed so that it has a constant projection on the array response $a_{BS}(\overline{\emptyset}_u)$, with $u$ in the range $\{65, \ldots, 127\}$ where $\overline{\emptyset}_u$ is in $\left\{\frac{2\pi 65}{256}, \frac{2\pi 66}{256}, \ldots, \frac{2\pi 128}{256}\right\}$, and zero projection on the other directions.

From the above description, we can say that the design of the beamforming vector $\left[F_{(s,k)}\right]_{:,m}$ is given as follows [22]

$$A_{BS,Dictionary} F_{(s,k)} = C_s G(s,k)$$

$$F_{(s,k)} = C_s \left(A_{BS,D} A_{BS,D}^H\right)^{-1} A_{BS,D} G(s,k)$$

where $D$ refers to the Dictionary, and $G(s,k)$ is an $N$ x $K$ matrix where each column $m$ has 1's in the locations $u, u \in \mathrm{I}_{(s,k,m)}$, and zeros in the locations $u, u \notin \mathrm{I}_{(s,k,m)}$. By using the design of hybrid beamforming as we described previously, the precoding matrix $F_{(s,k)}$ is defined as $F_{(s,k)} = F_{RF,(s,k)} F_{BB,(s,k)}$. Therefore, the design of the hybrid training precoding is given as follows [22]

$$\left\{ \mathbf{F}^{\star}_{\mathrm{RF},(s,k)}, \left[\mathbf{F}^{\star}_{\mathrm{BB},(s,k)}\right]_{:,m} \right\} =$$

$$\begin{aligned} \arg\min \quad & \| \left[\mathbf{F}_{(s,k)}\right]_{:,m} - \mathbf{F}_{\mathrm{RF},(s,k)} \left[\mathbf{F}_{\mathrm{BB},(s,k)}\right]_{:,m} \|_F, \\ \text{s.t.} \quad & \left[\mathbf{F}_{\mathrm{RF},(s,k)}\right]_{:,i} \in \left\{ [\mathbf{A}_{\mathrm{can}}]_{:,\ell} \mid 1 \le \ell \le N_{\mathrm{can}} \right\}, \\ & i = 1, 2, \ldots, N_{\mathrm{RF}} \\ & \|\mathbf{F}_{\mathrm{RF},(s,k)} \left[\mathbf{F}_{\mathrm{BB},(s,k)}\right]_{:,m} \|_F^2 = 1, \end{aligned}$$

where $\left[F_{(s,k)}\right]_{:,m} = C_s \left(A_{BS,D} A_{BS,D}^H\right)^{-1} A_{BS,D}[G(s,k)]_{:,m}$, and $A_{can}$ is a $N_{BS}$ x $N_{can}$ matrix which carries the candidate set of possible analog beamforming vectors with quantized bits. The columns of the candidate matrix can be chosen to meet the requirements of the analog beamforming constraints including the power constraint by setting $N_s = 1$.

In order to understand how the adaptive channel estimation works, the next sub-section explains these steps in more detail.

### 2.3.7 Adaptive Channel Estimation for Multipath mmW Channel

Because of the poor scattering nature of a mmW channel, only a small number of paths exist, say 3 or 4 paths [20][21]; therefore the sparse compressed sensing solution can be utilized to estimate the mmW channel. The channel estimation for multipath mmW channel at the BS is done in a similar way at the MS. In case multiple paths exist in the mmW channel between BS and MS, there is an algorithm proposed by [22] to estimate AODs/AOAs with associated path gains of the dominant paths of the channel. Because of the multiple paths case, the adaptive algorithm uses $KL_d$ precoding and measurement vectors between BS and MS instead of $K$, where $L_d$ is the number of the dominant paths in mmW channel. At each stage, the dominant paths are selected from the $KL_d$ partitions for more refinement by dividing the selected partition into $K$ smaller partitions in the next stages. In addition, the AODs/AOAs range is divided into $KL_d$ ranges at each stage. Therefore, the ranges $\mathrm{I}_{(k,s,m)}$ is given as follows [22]

$$\mathrm{I}_{(k,s,m)} = \left\{\frac{N}{K^s L_d}(K(k-1)+m-1)+1, \ldots, \frac{N}{K^s L_d}(K(k-1)+m)\right\}$$

where the quantized AODs/AOAs range associated with each beamforming vector $m$ , of subset $k$, of level $s$.

Algorithm 2.8 explains how to estimate the $L_d$ paths of mmW channel. In this algorithm, there are $L_d$ outer iterations, and in each one, only one path is detected after subtracting the trajectories of the previously detected paths. More precisely, the algorithm 2.8 operates as follows: In the first iteration, and in the first stage, both BS, and MS use $KL_d$ beamforming vectors, which are made by dividing the AODs and AOAs range at the BS and MS respectively. Then the algorithm selects the most dominant paths $L_d$ by selecting the maximum received signals power at each partition of each level $s$. This process is repeated until the last stage is reached with the required AOD/AOA resolution, and only one path is detected at this iteration. Then the trajectories used by the BS and MS to detect the first path are stored in the matrix $T^{BS}$ and $T^{MS}$ respectively to be used in later iteration. In the next iteration, the same precodings and measurements are repeated to detect one more path; however, at each stage of this iteration, the contribution of the first path that has been already detected in the previous iteration, which is stored in $T^{BS}$ and $T^{MS}$ matrix, is cancelled out before selecting the new AOD/AOA ranges for the BS and MS. Moreover, the new AOD/AOD ranges of each stage of this iteration are refined and selected by considering the ranges at the $T^{BS}$matrix at BS and $T^{MS}$matrix at MS in order to detect different paths with AODs/AOAs separated by a resolution up to $\frac{2\pi}{N}$. The algorithm moves to the next iteration to detect one more path by the same way until all $L_d$ paths are solved. After estimating the AODs/AOAs for all paths with the desired resolution, the algorithm finally calculates the estimated path gains by using a linear least squares estimator (LLSE).

The total number of adaptive stages needed by algorithm 2.8 to estimate the AoAs/AoDs of $L_d$ paths of the mmW channel with a resolution $\frac{2\pi}{N}$ is $L_d^2 \left\lceil \frac{KL_d}{N_{RF}} \right\rceil log_K(\frac{N}{L_d})$ .

Algorithm 2.8. Adaptive Estimation Algorithm for Multi-Path mmW Channels [22]

---

**Input:** BS and MS know $N, K, L_d$, and have $\mathcal{F}, \mathcal{W}$

**Initialization:** $\mathbf{T}^{\mathrm{BS}}_{(1,1)} = \{1, \ldots, 1\}, \mathbf{T}^{\mathrm{MS}}_{(1,1)} = \{1, \ldots, 1\}$

$\mathrm{S} = \log_K (N/L_d)$

**for** $\ell \leq L_d$ **do**

  **for** $s \leq \mathrm{S}$ **do**

    **for** $m_{\mathrm{BS}} \leq KL_d$ **do**

      BS uses $\left[\mathbf{F}_{(s,\mathbf{T}^{\mathrm{BS}}_{(\ell,s)})}\right]_{:,m_{\mathrm{BS}}}$

      **for** $m_{\mathrm{MS}} \leq KL_d$ **do**

        MS uses $\left[\mathbf{W}_{(s,\mathbf{T}^{\mathrm{BS}}_{(\ell,s)})}\right]_{:,m_{\mathrm{MS}}}$

        After MS measurements:

        $\mathbf{y}_{m_{\mathrm{BS}}} =$

        $\sqrt{P_s}\left[\mathbf{W}_{(s,\mathbf{T}^{\mathrm{MS}}_{(\ell,s)})}\right]\mathbf{H}\left[\mathbf{F}_{(s,\mathbf{T}^{\mathrm{BS}}_{(\ell,s)})}\right]_{:,m_{\mathrm{BS}}} + \mathbf{n}_{m_{\mathrm{BS}}}$

    $\mathbf{y}_{(s)} = [\mathbf{y}_1^T, \mathbf{y}_2^T, \ldots, \mathbf{y}_K^T]^T$

    **for** $p = 1 \leq \ell - 1$ **do**

      Project out previous path contributions

      $\mathbf{g} = \mathbf{F}^T_{(s,\mathbf{T}^{\mathrm{BS}}_{(p,s)})}\left[\mathbf{A}_{\mathrm{BS,D}}\right]^*_{:,\mathbf{T}^{\mathrm{BS}}_{(p,s)}(1)} \otimes$

        $\mathbf{W}^H_{(s,\mathbf{T}^{\mathrm{MS}}_{(p,s)})}\left[\mathbf{A}_{\mathrm{MS,D}}\right]_{:,\mathbf{T}^{\mathrm{MS}}_{(p,s)}(1)}$

      $\mathbf{y}_{(s)} = \mathbf{y}_{(s)} - \mathbf{y}^H_{(s)}\mathbf{g}\left(\mathbf{g}^H\mathbf{g}\right)\mathbf{g}$

    $\mathbf{Y} = \mathrm{matix}(\mathbf{y}_{(s)})$ Return $\mathbf{y}_{(s)}$ to the matrix form

    $(m^\star_{\mathrm{BS}}, m^\star_{\mathrm{MS}}) = \underset{\forall m_{\mathrm{BS}}, m_{\mathrm{MS}} = 1,2,\ldots,K}{\arg\max} \left[\mathbf{Y} \odot \mathbf{Y}^*\right]_{m_{\mathrm{MS}}, m_{\mathrm{BS}}}$

    $\mathbf{T}^{\mathrm{BS}}_{(\ell,s+1)}(1) = K(m^\star_{\mathrm{BS}} - 1) + 1$

    $\mathbf{T}^{\mathrm{MS}}_{(\ell,s+1)}(1) = K(m^\star_{\mathrm{MS}} - 1) + 1$

    **for** $p = 1 \leq \ell - 1$ **do**

      $\mathbf{T}^{\mathrm{BS}}_{(\ell,s+1)}(p) = \mathbf{T}^{\mathrm{BS}}_{(p,s+1)}(1)$

      $\mathbf{T}^{\mathrm{MS}}_{(\ell,s+1)}(p) = \mathbf{T}^{\mathrm{MS}}_{(p,s+1)}(1)$

$\hat{\phi}_\ell = \bar{\phi}_{\mathbf{T}^{\mathrm{BS}}_{(\ell,\mathrm{S}+1)}(1)}, \hat{\theta}_\ell = \bar{\theta}_{\mathbf{T}^{\mathrm{MS}}_{(\ell,\mathrm{S}+1)}(1)}$

$\mathbf{g} = \mathbf{F}^T_{(\mathrm{S},\mathbf{T}^{\mathrm{BS}}_{(\ell,\mathrm{S})})}\left[\mathbf{A}^*_{\mathrm{BS,D}}\right]_{:,\mathbf{T}^{\mathrm{BS}}_{(\ell,\mathrm{S}+1)}(1)} \otimes$

$\mathbf{W}^H_{(\mathrm{S},\mathbf{T}^{\mathrm{MS}}_{(\ell,\mathrm{S})})}\left[\mathbf{A}_{\mathrm{MS,D}}\right]_{:,\mathbf{T}^{\mathrm{MS}}_{(\ell,\mathrm{S}+1)}(1)}$

$\hat{\alpha}_\ell = \sqrt{\rho/P_{(\mathrm{S})}G_{(\mathrm{S})}}\mathbf{y}^H_{(\mathrm{S})}\mathbf{g}/\mathbf{g}^H\mathbf{g}$

---

Chapter 3

# Simulation Results

## 3.1 Introduction

This chapter provides simulation results about the performance of classical MIMO, uplink and downlink massive MIMO, and the downlink mmW massive MIMO systems. We provide the simulation results of the Alamouti code implemented in classical MIMO, detection algorithms and simulated sum rate done for uplink and downlink massive MIMO, and Alamouti code and detection algorithms (Maximum Likelihood and MMSE detections) for the downlink mmW massive MIMO systems. The implementation of the simulator was done using Matlab software. In order to ensure sufficient reliability of the bit error rate curves, most of the simulation points were run until 60 errors were obtained or $10^7$ transmitted bits were reached. For all detection algorithms, QPSK modulation is used without any coding scheme. Alamouti code is implemented with BPSK and QPSK modulation for classical MIMO, and only QPSK for the downlink mmW massive MIMO systems.

## 3.2 Performance of Alamouti Code

In this section, simulation results are provided for the performance of the Alamouti code which was described in Chapter 2. The information source is divided into blocks of bits. Then, by using a given modulation scheme, $K$ symbols are picked from the constellation. These symbols are used in the generator matrix of the Alamouti code to generate the codewords. After that, the elements of $t\ th$ row of the codeword are transmitted from different antennas at time slot $t$. We consider the small-scale variations only without large-scale variations to model the fading

channel. We also assume a quasi-static flat Rayleigh fading model for the channel. Therefore, the path gains are fixed during the transmission of one block. The receiver uses Maximum Likelihood decoding with perfect knowledge of the channel to detect the transmitted symbols and bits. Then, we show the bit error rate (BER) versus the received $\frac{E_b}{N_0} dB$.

Figure 3.1 provides results for BPSK modulation using different numbers of receive and transmit antennas. For a single transmit antenna and receive antenna (SISO), the given modulation is used with no coding. For two transmit antennas with one (2x1), and two receive antennas (2x2), the given modulation and Alamouti code are used. We further assume that the total transmit power from the two transmit antennas is the same as the transmit power from the single transmit antenna to make the comparison fair. In this case, we have three scenarios: in the first one, there is no diversity by utilizing one transmit and receive antenna. In the second and third scenarios, there is an order of two and four diversity and full rate, $R = 1$ for 2x1 and 2x2 Alamouti STBCs respectively.

As we can see in Figure 3.1, the performance of the Alamouti code with two transmit and receive antennas is much better than the Alamouti code with two transmit antennas and a single receive antenna, or the single transmitter and single receiver (SISO), which has no diversity. It is seen that at a bit error probability of $10^{-4}$, the 2x2 Alamouti code provides about 9 $dB$ gain over the 2x1 Alamouti code. Therefore, by increasing the number of receive antennas to two, we can obtain a better BER because of the increase of the diversity from two to four.

Figure 3.2 displays BER values against $\frac{E_b}{N_0}$ values for the QPSK modulation scheme with Alamouti STBCs. As can be seen from the plot, 2x2 Alamouti STBC has the smallest BER values for all $\frac{E_b}{N_0} dB$ values. This result is expected because the 2x2 Alamouti system has one

more receiver when compared with the 2x1 Alamouti system and because of this additional receiver, its diversity is increased. SISO system has the highest BER values for all $\frac{E_b}{N_0}$ values because of no diversity.

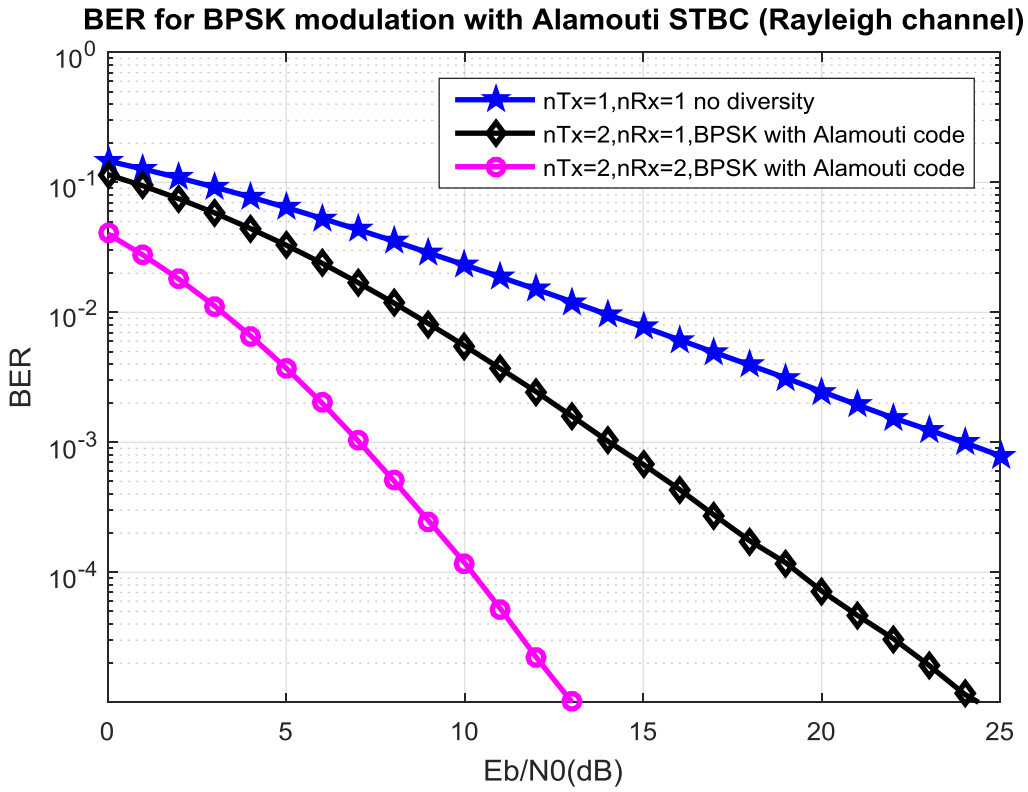


Figure 3.1. Bit error rate plotted against $\frac{E_b}{N_0}$ for BPSK modulation with Alamouti code at 1 bit/(s Hz), with different number of antennas at the transmitter and receiver.

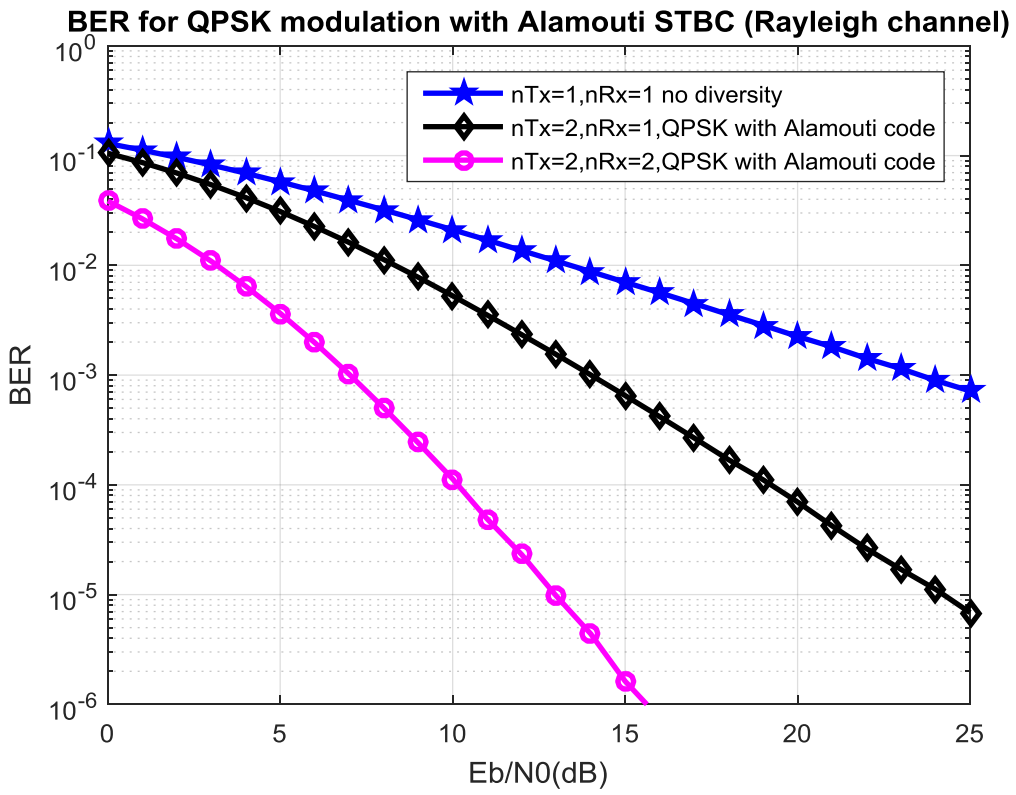


Figure 3.2. Bit error rate plotted against $\frac{E_b}{N_0}$ for QPSK modulation with Alamouti code at 2 bit/(s Hz), with different number of antennas at the transmitter and receiver.

## 3.3 Uplink and Downlink Performance of a Single-Cell Massive Multi User MIMO Systems.

In this section, we provide a set of performance results for uncoded QPSK uplink and downlink transmission in the lower frequency bands with different numbers of BS antennas, $N_t$, serving $K = 10$ users. The channel is also considered here to be a quasi-static flat Rayleigh fading and it is modeled by small-scale fading only, not considering large-scale variations. Because for a small cell, the distance is small enough so large-scale variation can be ignored. In addition, the BS has a perfect knowledge of the channel to detect and precode the data. The following performance results show the bit error rate (BER) versus the received $\frac{E_b}{N_0} dB$.

Figure 3.3 shows the BER performance results for uplink and downlink transmission with $N_t = 50$ and $K = 10$. The performance of the MRC/MRT, ZF, and MMSE are compared to each other. As can be seen from the plot, MMSE and ZF detector/precoder perform significantly better than MRC/MRT over the higher range of $\frac{E_b}{N_0}$ . Due to their sensitivity to multi user interference, MRC/MRT has the worst performance over the higher range of $\frac{E_b}{N_0}$. In the lower $\frac{E_b}{N_0}$ regime, MRC/MRT performs similarly to the other schemes. The overall BER performance of the downlink transmission is worse than the uplink one due to the normalization constant chosen to satisfy the specific power constraint. However, a bit error probability of $10^{-6}$ can be obtained with $\frac{E_b}{N_0} \approx 5\ dB$ only using either ZF or MMSE precoder for the downlink transmission.

When $N_t \gg K$, both the multi user interference and the fading effects tend to disappear, which gives clear insight about the favorable environments. Consequently, the BER performance for the massive MU-MIMO $N_t$x $K$ is improved as can be seen in Figure 3.4.

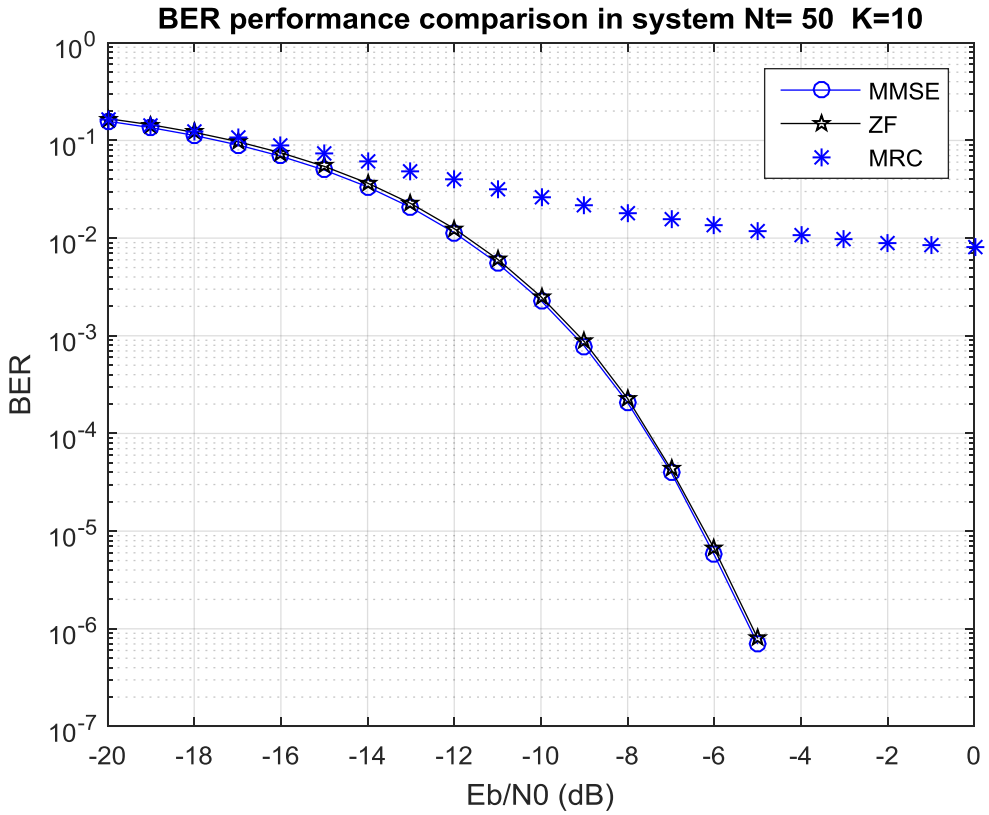


(a) Uplink transmission

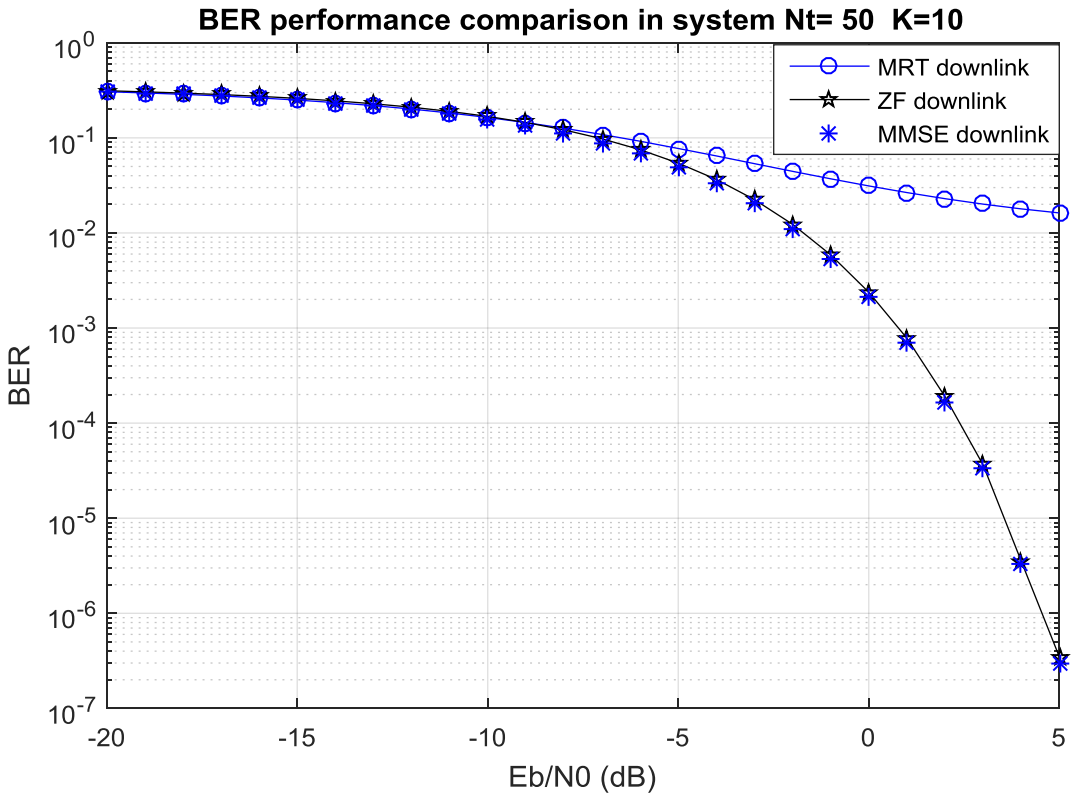


(b) Downlink transmission

Figure 3.3 BER performance for QPSK massive MU-MIMO on uplink and downlink transmission with $K$ = 10 and $N_t$ = 50.

Figure 3.4 shows the BER performance results for $N_t$ = 250 and $K$ = 10 massive MU-MIMO. As we can see from the plot, the performance penalty caused by MRC/MRT compared to MMSE and ZF detector/precoder can be made quite small, by increasing $N_t$ significantly. The plot shows that with $N_t = 250$ , the MRC/MRT can approximate the other schemes.

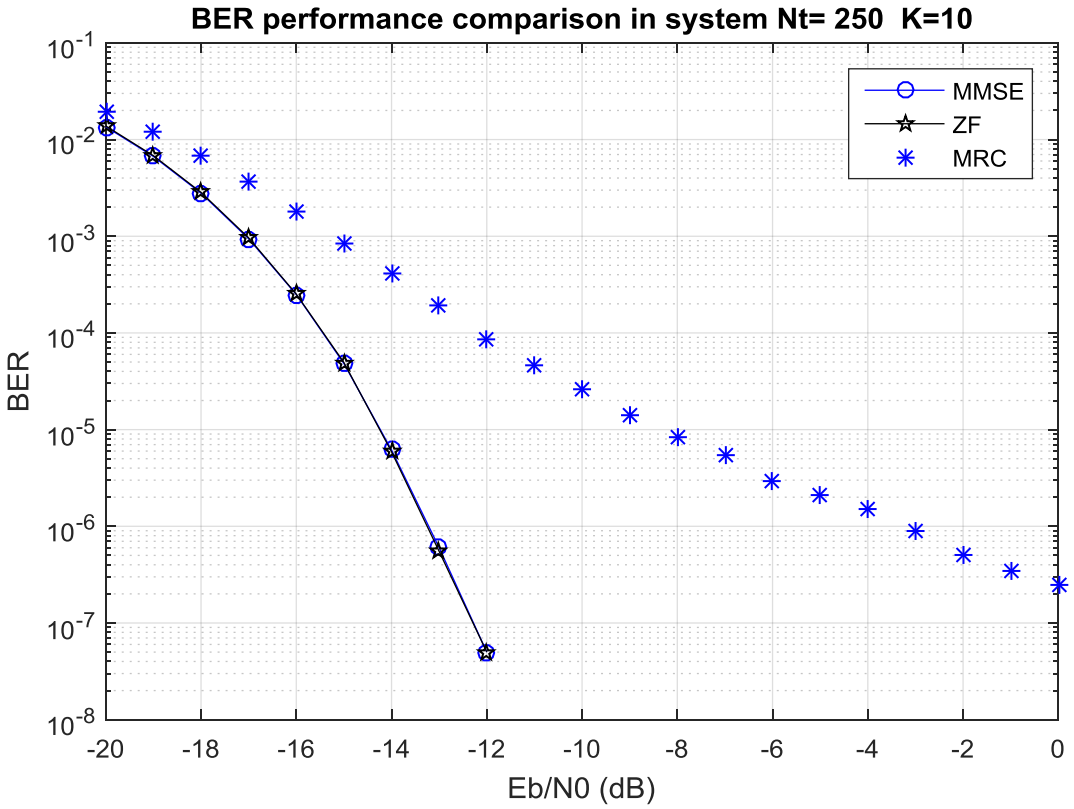


(a) Uplink transmission

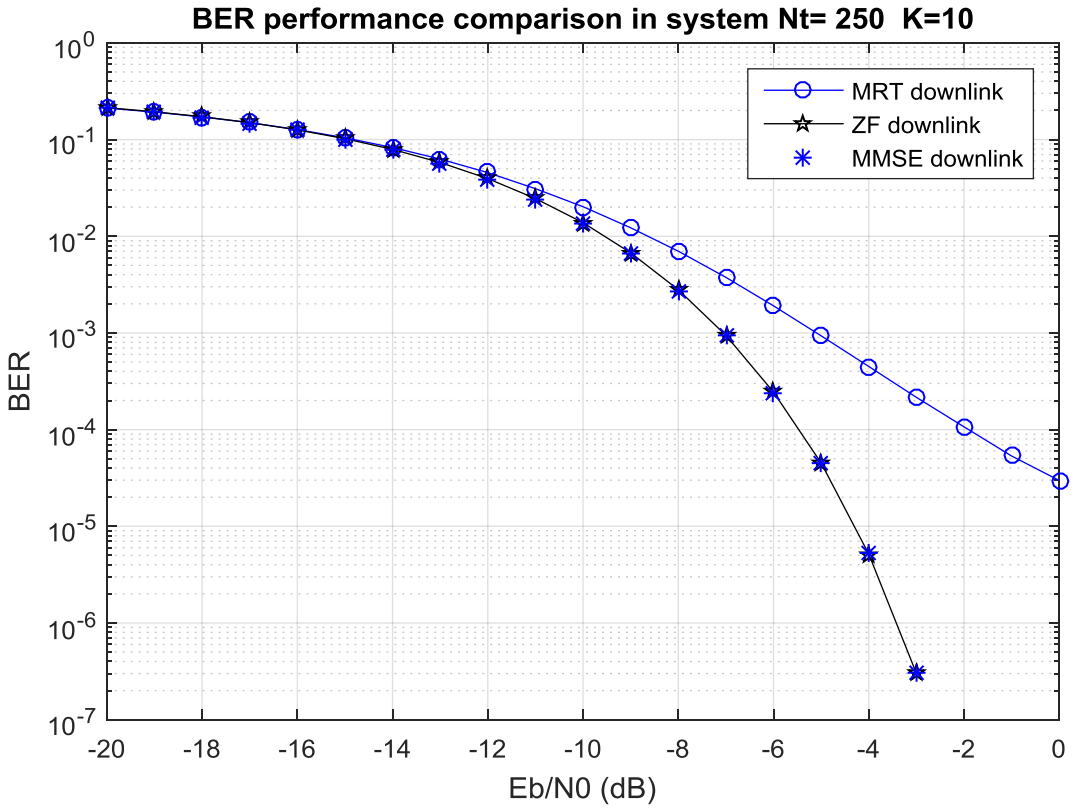


(b) Downlink transmission

Figure 3.4 BER performance for QPSK massive MU-MIMO on uplink and downlink transmission with $K$ = 10 and $N_t$ = 250.

It is seen from the plot that for a bit error probability of $10^{-6}$ on the uplink transmission, the $250 \times 10$ massive MU-MIMO provides about $8\,dB$ gain over the use of the $50 \times 10$ uplink massive MU-MIMO system. In addition, for a bit error probability of $10^{-6}$ on the downlink transmission, the $250 \times 10$ massive MU-MIMO provides also about $8\,dB$ gain over the $50 \times 10$ downlink.

Although the MRC/MRT requires the lowest complexity among the detectors and precoders, it performs poorly; therefore, its use should be avoided in favor of the other detectors and precoders such as ZF and MMSE. However, if the values of BER obtained by MRC/MRT is

acceptable, with highly increased $N_t$, it is better to use MRC/MRT due to its lower complexity compared to the ZF and MMSE detector/precoder.

### 3.3.1 The Simulated Sum Rate for Uplink and Downlink Transmission of Single-Cell Massive Multi User MIMO Systems.

The simulated sum rate $R$ for QPSK uplink and downlink transmission in the lower frequency bands for $50 \text{ x } 10$ and $250 \text{ x } 10$ massive multi user MIMO systems is provided in this section using the expression of $R$ given in Section 2.2. Figures 3.5 and 3.6 show the results of the simulated sum rate versus the received $SNR\ dB$.

As can be seen from the plots, a single-cell $250 \text{ x } 10$ uplink and downlink massive multi user MIMO systems has the highest sum rate values for all $SNR\ dB$ values. This result is expected because of the rich scattering environment with $250 \text{ x } 10$ massive MU-MIMO systems. It is observed that, for higher SNR values the ZF and MMSE attain a higher sum-rate than the MRC/MRT for all cases. However, the MRC/MRT is still able to obtain the same sum rate as the other schemes for lower SNR values. It is observed also that the low complexity MRC/MRT performance can be improved by increasing $N_t$ to 250 antennas. Therefore, we conclude that as the number of BS antennas increases, the achievable sum rate for each scheme also increases. It can also be seen from the plots that the achievable rate is higher than the number of mobile users, which means that more than 1 bit per second per Hertz is achieved for each user. In conclusion, ZF and MMSE are more power efficient than MRT to achieve a high data rate.

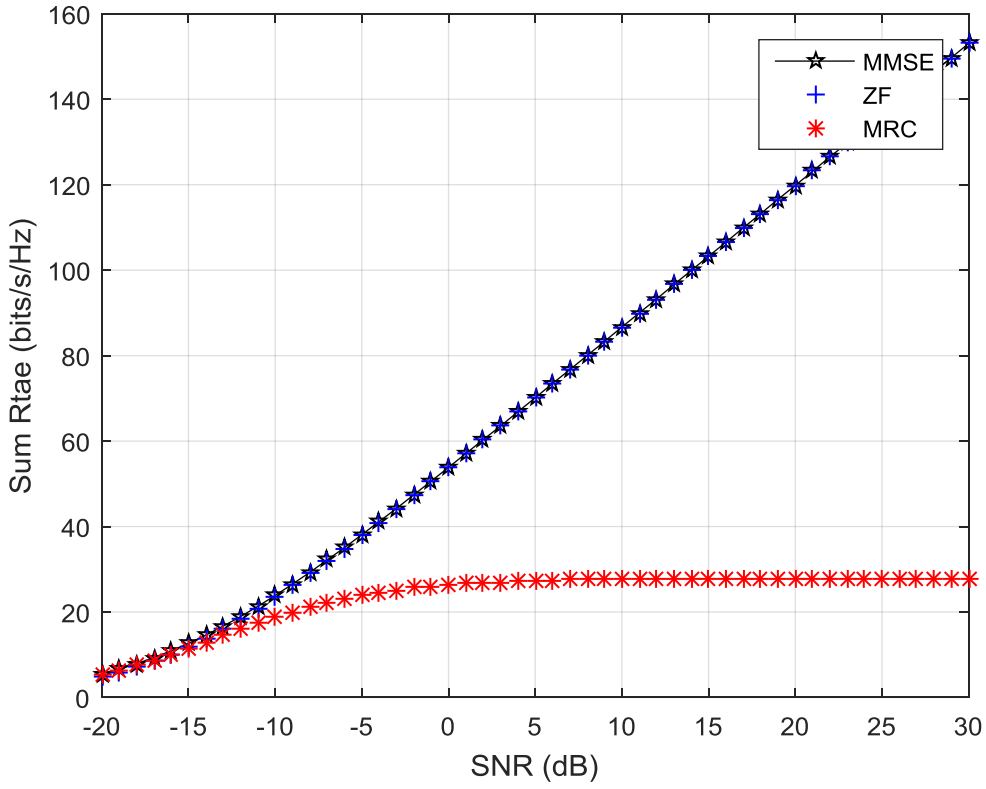


(a) Uplink transmission

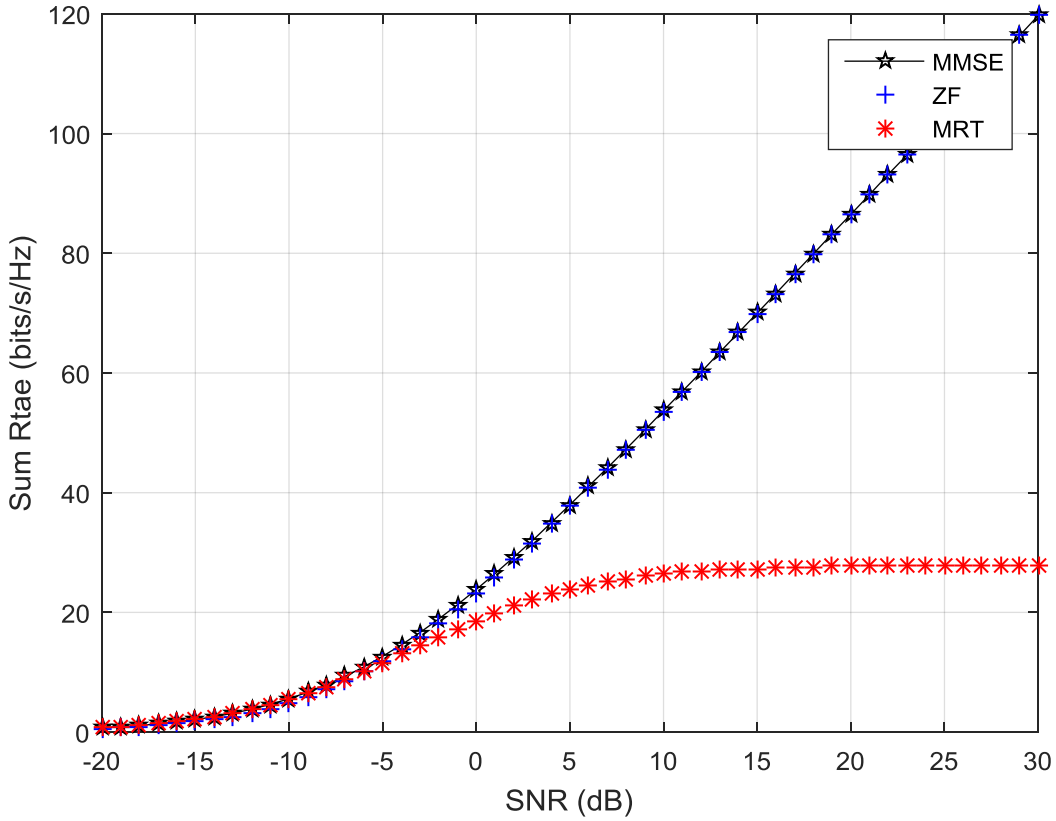


(b) Downlink transmission

Figure 3.5 Downlink and uplink sum-rate versus SNR dB for $K$ = 10 and $N_t$ = 50 massive MU-MIMO systems.

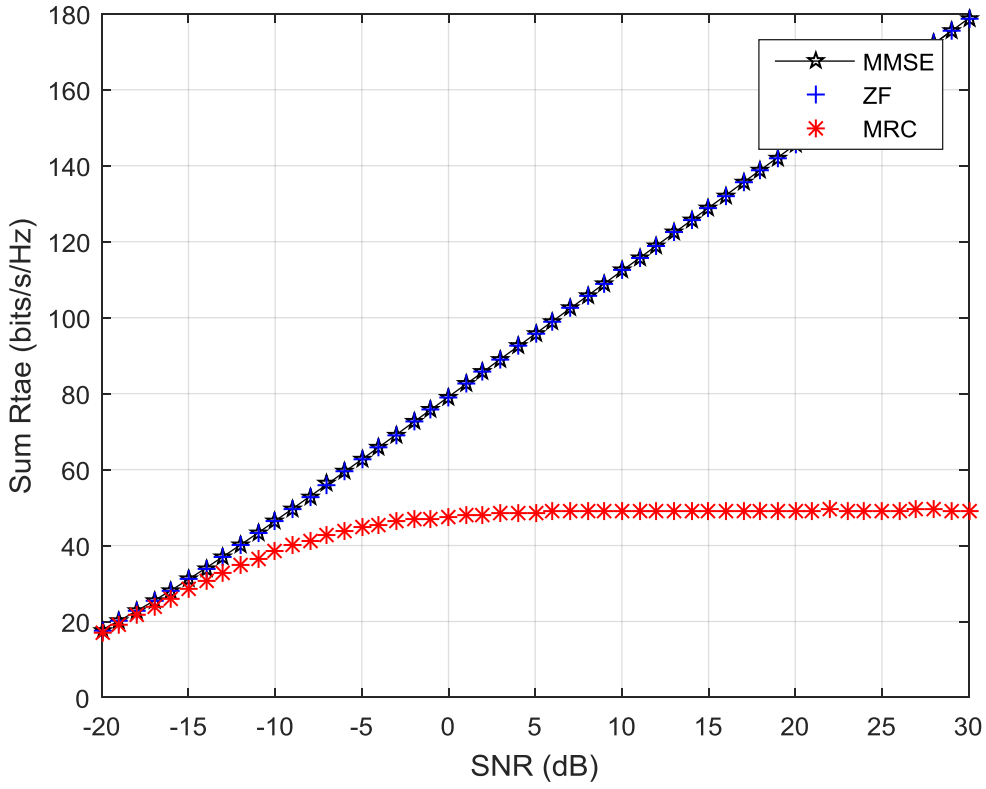


(a) Uplink transmission

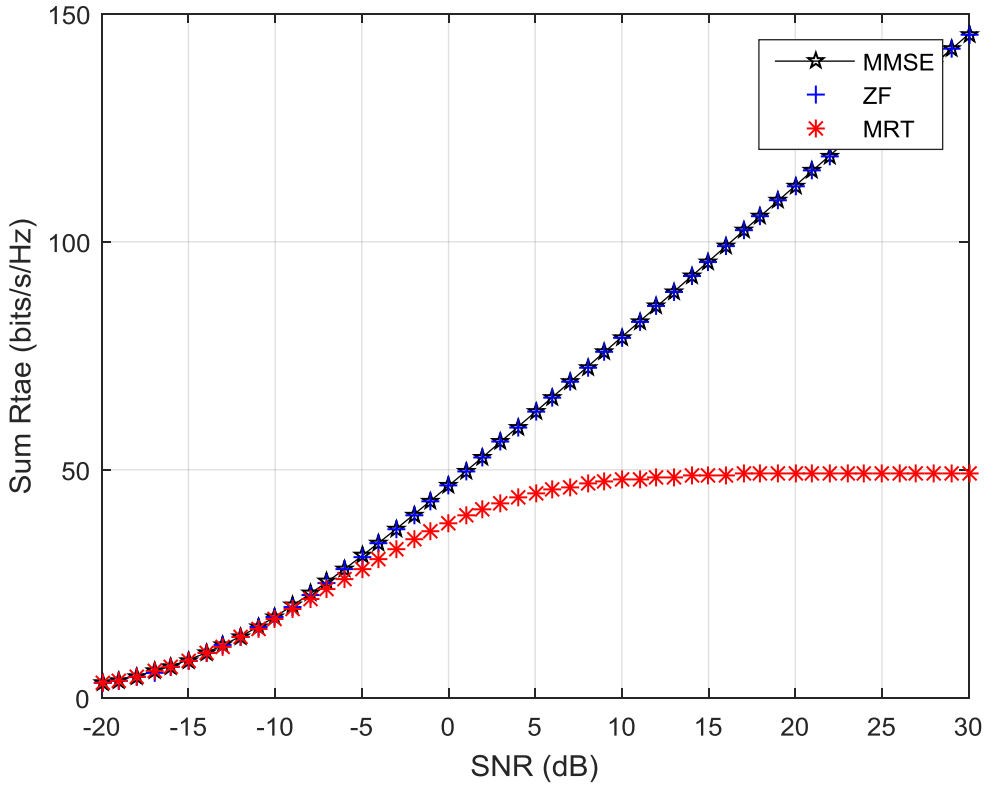


(b) Downlink transmission

Figure 3.6 Downlink and uplink sum-rate versus SNR dB for $K$ = 10 and $N_t$ = 250 massive MU-MIMO systems.

## 3.4 Downlink Performance of a Single-Cell Hybrid Beamforming MmW Massive MIMO Systems.

In this section, we present numerical results to evaluate the performance of ML, MMSE, combined system, and Alamouti code for uncoded downlink transmission in mmW frequency bands with different numbers of data streams, RF chains, and MS antennas. The combined system has been described in Hybrid Beamforming Solution in Section 2.3.2. In addition, we use QPSK modulation for the MMSE, ML detectors and combined system in the case of $N_S$ =

2 and 3; however, in order to make fair comparison between the Alamouti code and the other schemes, we use BPSK modulation for the MMSE, ML detectors and combined system in the case of $N_S = 2$ and QPSK modulation for the $N_S = 2$ Alamouti code as we will explain later. In these simulations, we adopt the hybrid analog/digital system architecture presented in Fig 2.4, considering the case where there is only one BS and one MS at a distance of 100 meters. We make the number of data streams $N_S$ equal to the number of mmW channel paths $L$ for all scenarios, $N_S = L$. The antenna arrays are ULAs, and the spacing between antenna elements is equal to $\lambda/2$. The RF phase shifters are assumed to have only 7 quantization bits. The system is assumed to operate at 28 GHz carrier frequency, has a bandwidth of 100 MHz, and with path loss exponent $n = 3.4$. We use the channel model which is described in Section 2.3.2, with $\overline{P_R} = 1$, and the number of paths $L = 3$ in the case of $N_S = 3$ and $L = 2$ for $N_S = 2$. The azimuth AOAs/AODs are assumed to be uniformly distributed between $[0,2\pi]$. The BS channel estimation is done with AOA/AOD resolution parameter $N = 192$ and beamforming vectors $K = 2$ for $N_S = L = 3$ and with AOA/AOD resolution parameter $N = 162$ and beamforming vectors $K = 3$ for $N_S = L = 2$ as discussed in Section 2.3.7. The hybrid precoding/combining matrices are constructed as we described in Section 2.3.4.

In the simulations in Section 3.4.1 to 3.4.3, we use the hybrid precoder and hybrid combiner for channel estimation which was described in Section 2.3.7. We then use the hybrid precoder to precode the data streams to MS in the downlink transmission using the estimated channel; after that we use the hybrid combiner, assuming a perfect channel at MS to combine the data streams. Moreover, after combining the received signal (combined system), the ML, MMSE detectors, and the Alamouti code use the effective channel as we described in Hybrid Beamforming Solution in Section 2.3.2 to detect the data streams. We also present numerical results in Section

3.4.4 to evaluate the downlink performance of hybrid beamforming mmW massive MIMO systems by assuming a perfect channel state information at both MS and BS and using the effective channel at MS to detect the data streams.

### 3.4.1 Performance Evaluation of ML and MMSE Detectors for Multiple Data Streams $N_S = \mathrm{L} = 3$.

In this simulation, the number of data streams $N_S$ and mmW channel paths L is equal to 3. First, we evaluate the case when the BS has $N_{BS} = 64$ antennas, and 10 RF chains, the MS has $N_{MS} = 32$ antennas and 6 RF chains. Then, we keep the same number of BS and MS antennas but with 3 RF chains at both sides.

Figure 3.7 shows the BER performance results for QPSK hybrid beamforming mmW massive MIMO system on downlink transmission for $N_{BS} = 64$ and $N_{MS} = 32$ with 10 and 6 RF chains respectively. We compare the performance of MMSE detector, ML detector and combined system at the MS. As can be seen from the plot, the ML and MMSE detectors perform better than the combined system over all range of $\frac{E_b}{N_0}$. Moreover, the ML detector achieves the smallest BER values over the higher range of $\frac{E_b}{N_0}$ ; however, the ML and MMSE detectors perform similarly over the lower range (approximately from -30 to -15 dB) of $\frac{E_b}{N_0}$. A bit error probability of $10^{-2}$ can be obtained with $\frac{E_b}{N_0} = 8\ dB$ using the ML detector; whereas the MMSE detector needs about $26\ dB$ which is significantly higher, with a $18\ dB$ gain to obtain the same BER.

Now, let us consider that we have the same number of BS and MS antennas but with 3 RF chains at both sides. Note that the number of data streams $N_s \leq N_{RF}$, the number of RF chains as we explained in Hybrid Beamforming Solution in Section 2.3.2. As can be seen from Figure 3.8,

the ML and MMSE detectors still perform better than the combined system over all range of $\frac{E_b}{N_0}$. Moreover, the ML detector still achieves the smallest BER values over the higher range of $\frac{E_b}{N_0}$ and performs similarly as the MMSE detector over the lower range (approximately from -30 to -20 dB) of $\frac{Eb}{N0}$. A bit error probability of $10^{-2}$ can be obtained with $\frac{E_b}{N_0} = 15\ dB$ using the ML detector; whereas the MMSE detector needs more than $30\ dB$ to obtain the same BER.

By comparing the results from both Figures 3.7 and 3.8, it is observed that the performance of 10 and 6 RF chains ML detector as shown in Figure 3.7 outperforms the performance of 3 RF chains ML as can be seen in Figure 3.8 by $7\ dB$ and $5\ dB$ at a bit error probability of $10^{-2}$ and $10^{-3}$ respectively . Also, the performance of 10 and 6 RF chains MMSE detector as shown in Figure 3.7 is superior to the performance of 3 RF chains MMSE from Figure 3.8 with about $19\ dB$ gain at a bit error probability of $10^{-1}$.

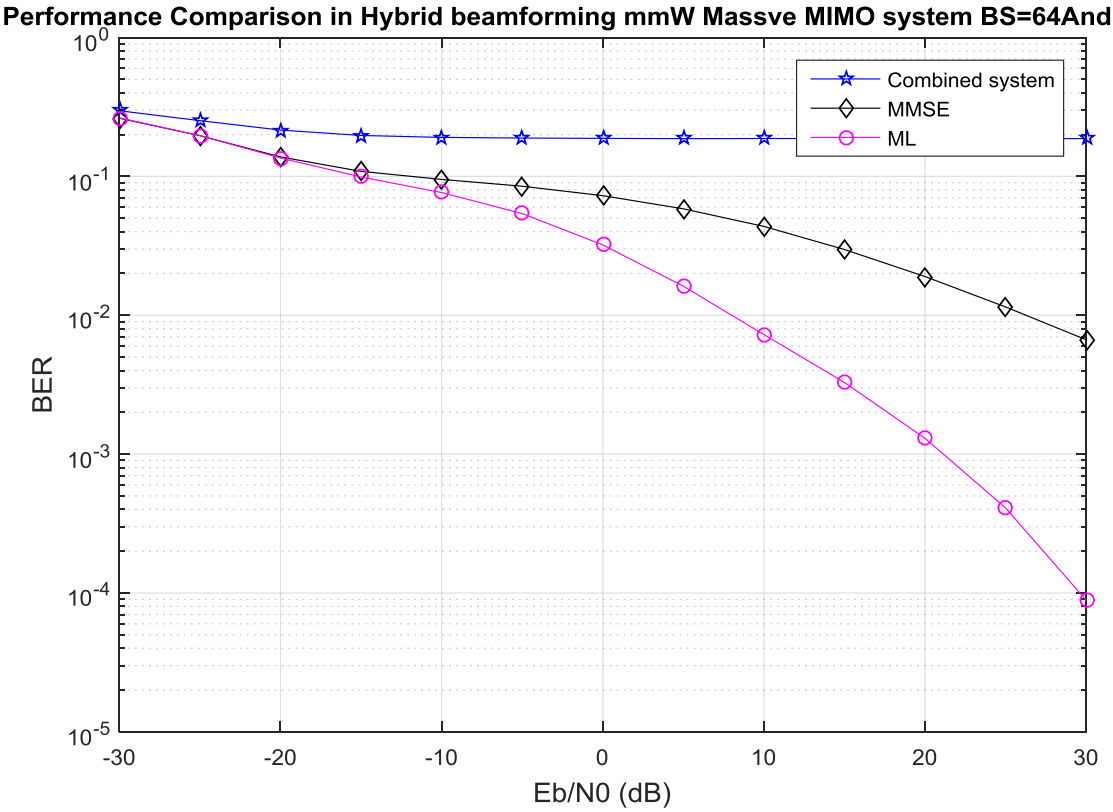


Figure 3.7. BER performance for uncoded QPSK single-cell hybrid beamforming mmW massive MIMO system on downlink transmission for $N_{BS} = 64$ and $N_{MS} = 32$ with 10 and 6 RF chains respectively, with $N_S = \mathrm{L} = 3$ at AOA/AOD resolution parameter $N = 192$ and beamforming vectors $K = 2$.

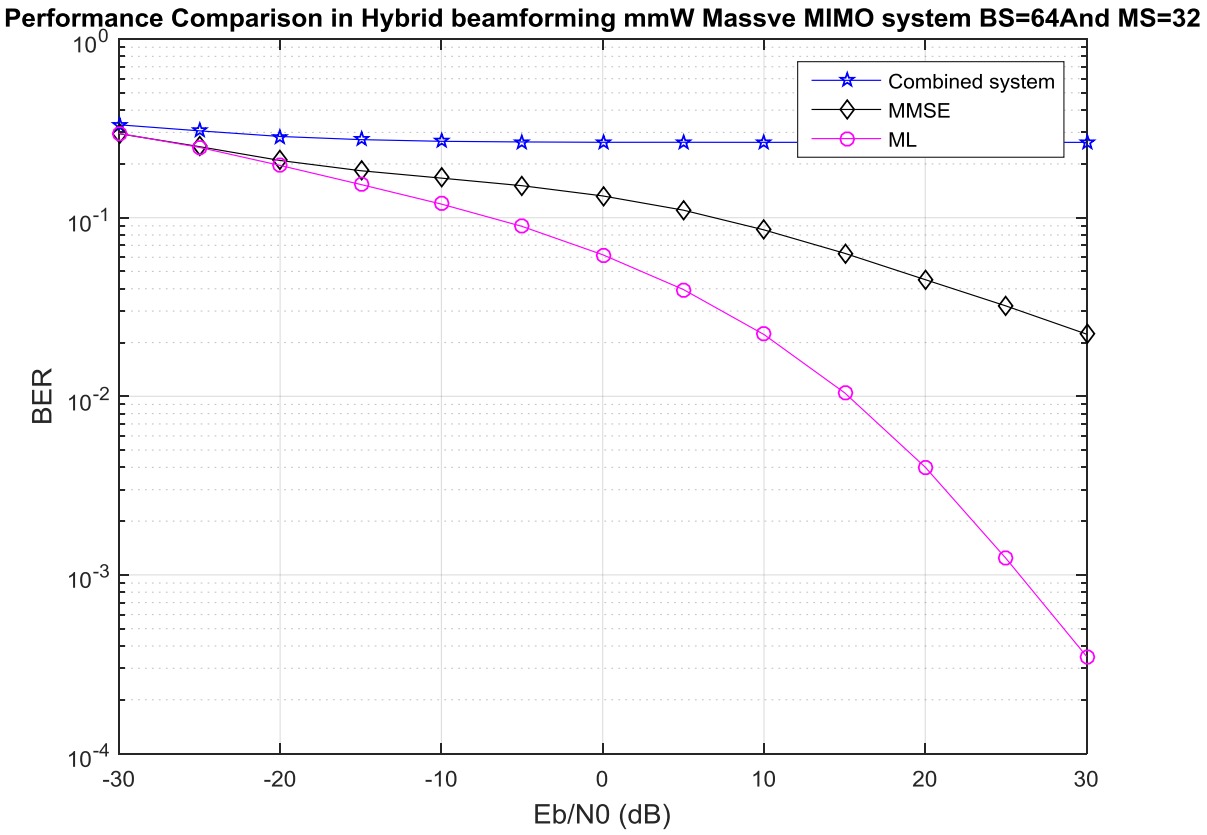


Figure 3.8. BER performance for uncoded QPSK single-cell hybrid beamforming mmW massive MIMO system on downlink transmission for $N_{BS} = 64$ and $N_{MS} = 32$ with 3 RF chains at both sides and $N_S = \mathrm{L} = 3$ at AOA/AOD resolution parameter $N = 192$ and beamforming vectors $K = 2$.

## 3.4.2 Performance Evaluation of ML and MMSE Detectors for Multiple Data Streams $N_S = \mathrm{L} = 2$.

In this simulation, we assume that the channel paths $L = 2$, and we reduce the number of data streams to two. In the first simulation of this section we still keep the same number of antennas and RF chains where the BS has $N_{BS} = 64$ antennas, and 10 RF chains, the MS has $N_{MS} = 32$

antennas and 6 RF chains. Then, we keep the same number of BS and MS antennas but with 3 RF chains at both sides.

Figure 3.9 shows the BER performance results for downlink transmission. The comparison is done between the ML detector, MMSE detector, and the combined system. As can be seen from the plot, the overall performance is similar to the previous result in Figure 3.7 where the ML and MMSE have the smaller BER values over the total range of $\frac{E_b}{N_0}$. In addition, the ML detector still achieves the smallest BER values over the higher range of $\frac{E_b}{N_0}$ , and performs similarly to the MMSE detector over the lower range (approximately from -30 to -20 dB) of $\frac{E_b}{N_0}$. As can be seen from Figure 3.9, the ML detector still outperforms the MMSE detector over the higher range of $\frac{E_b}{N_0}$. It is observed that for a bit error probability of $10^{-2}$, and $10^{-3}$ the ML detector provides about $13\ dB$ and more than $6\ dB$ gains respectively over the MMSE.

Now, let us consider the case when we have the same number of BS and MS antennas but with 3 RF chains at both sides. As can be seen from Figure 3.10, the 3 RF chains ML and MMSE still perform better than the 3 RF chains combined system over all range of $\frac{E_b}{N_0}$ , but with higher BER compared to the results obtained in Figure 3.9 where 10 and 6 RF chains are used at both BS and MS, respectively. Moreover, the ML detector still achieves the smallest BER values over the higher range of $\frac{E_b}{N_0}$ and performs similarly to the MMSE detector over the lower (approximately from -30 to -20 dB) range of $\frac{E_b}{N_0}$. A bit error probability of $10^{-2}$ can be obtained with $\frac{E_b}{N_0} = 17\ dB$ using the ML detector; whereas the MMSE detector needs about $30\ dB$ which is quite higher to obtain the same BER.

By comparing the results from both Figures 3.10 and 3.9, it is observed that the performance of 10 and 6 RF chains ML detector as shown in Figure 3.9 is better than the performance of 3 RF chains ML one as can be seen in Figure 3.10 with 7 $dB$ and 3 $dB$ gains at a bit error probability of $10^{-2}$ and $10^{-3}$ respectively. Also, the 10 and 6 RF chains MMSE detector as shown in Figure 3.9 outperforms the 3 RF chains MMSE from Figure 3.10 with about 7 $dB$ gain at a bit error probability of $10^{-2}$.

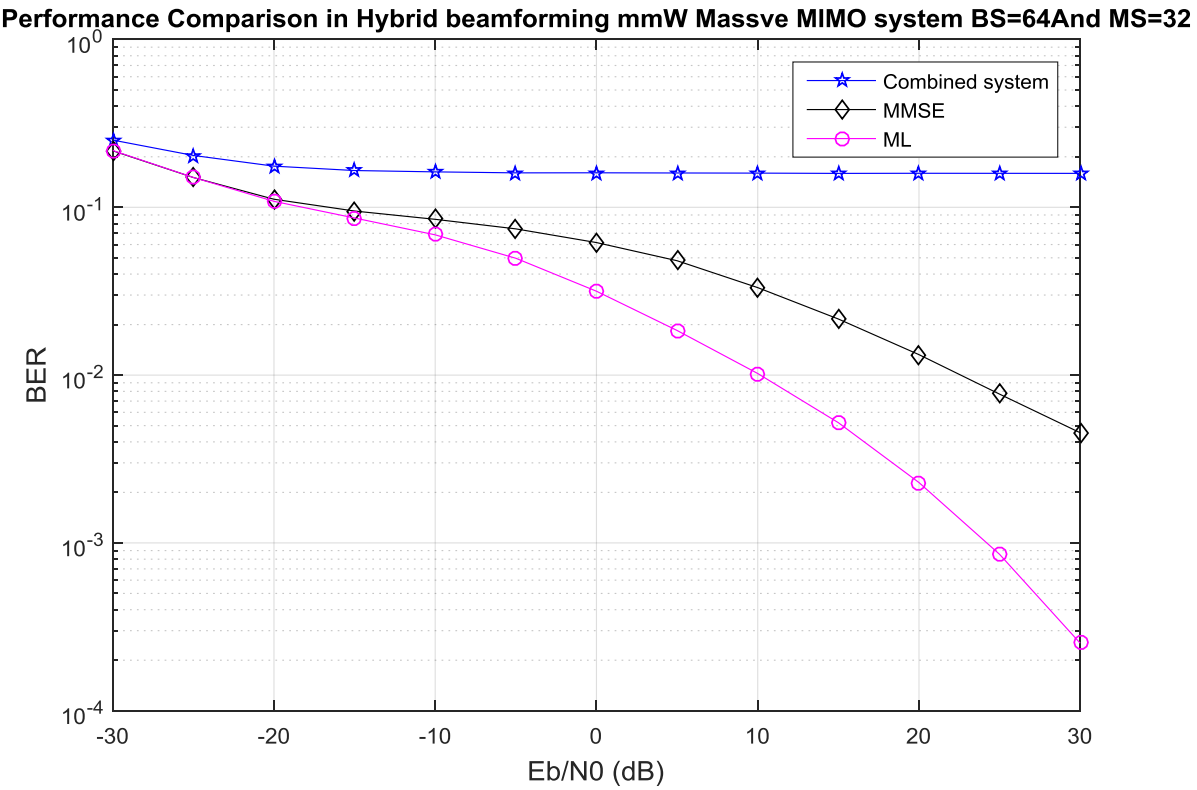


Figure 3.9. BER performance for uncoded QPSK single-cell hybrid beamforming mmW massive MIMO system on downlink transmission for $N_{BS} = 64$ and $N_{MS} = 32$ with 10 and 6 RF chains respectively, with $N_S = \mathrm{L} = 2$ at AOA/AOD resolution parameter $N = 162$ and beamforming vectors $K = 3$.

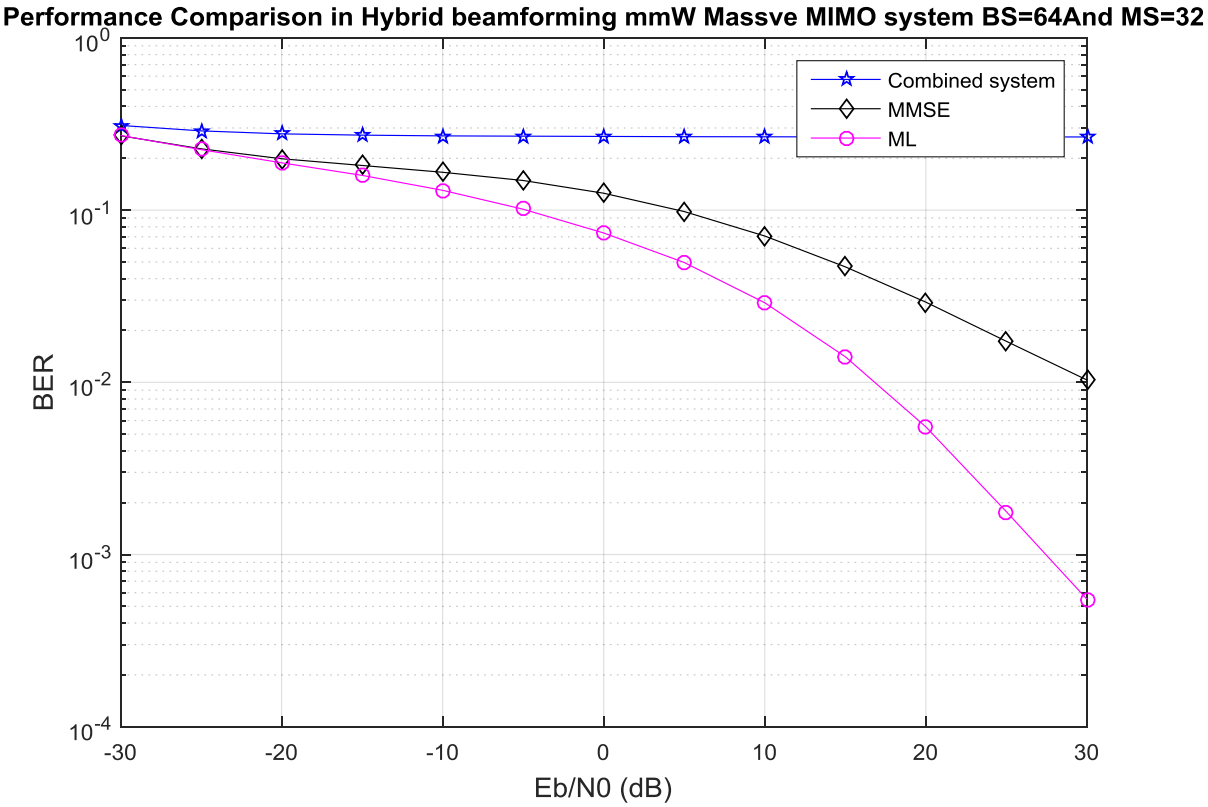


Figure 3.10. BER performance for uncoded QPSK single-cell hybrid beamforming mmW massive MIMO system on downlink transmission for $N_{BS} = 64$ and $N_{MS} = 32$ with 3 RF chains at both sides and $N_S = \mathrm{L} = 2$ at AOA/AOD resolution parameter $N = 162$ and beamforming vectors $K = 3$.

### 3.4.3 Performance Evaluation of the ML and MMSE Detectors for Multiple Data Streams $N_S = \mathrm{L} = 2$, and Alamouti Code for Multiple Data Streams $N_S = \mathrm{L} = 2$.

In this simulation, we have two data streams used by the MMSE, ML detectors, combined system, and Alamouti code. In addition, in the first simulation the BS has $N_{BS} = 64$ antennas, and 10 RF chains, the MS has $N_{MS} = 32$ antennas and 6 RF chains. Then, we keep the same number of BS and MS antennas but with 3 RF chains at both sides.

Figure 3.11 and 3.12 show the results for a spectral efficiency of 4 bits per channel use, i.e., we use QPSK modulation for the Alamouti code but BPSK modulation for the MMSE, ML detectors and combined system. This follows from the fact that the MMSE, ML detectors and combined system achieve a rate of 4 bits in two time slots and the Alamouti codes achieves a rate of 4 bits in two time slots as well to make a fair comparison between all systems. We consider that the MS in all cases receives the same number of bits per channel use. In addition, the mmW channel remains constant during the two time slots.

As can be seen from Figure 3.11, the Alamouti code achieves the smallest BER values over the total range of $\frac{E_b}{N_0}$; the combined system has the highest ones. In addition, the ML detector performs better than the MMSE over the total range of $\frac{E_b}{N_0}$; at a bit error probability of $10^{-2}$ the ML detector provides more than 9 $dB$ gain over the MMSE.

Moreover, as shown in Figure 3.11, the Alamouti code outperforms the other schemes including the combined system. In particular, at a bit error rate of $10^{-2}$, the performance improvements compared to the ML and MMSE detectors are nearly 19 $dB$ and more than 28 $dB$ respectively. In addition, at a bit error rate of $10^{-3}$, the Alamouti code needs approximately $\frac{E_b}{N_0} = 14\ dB$ whereas the other detectors need more than 20 $dB$ which is quite higher to achieve this bit error rate.

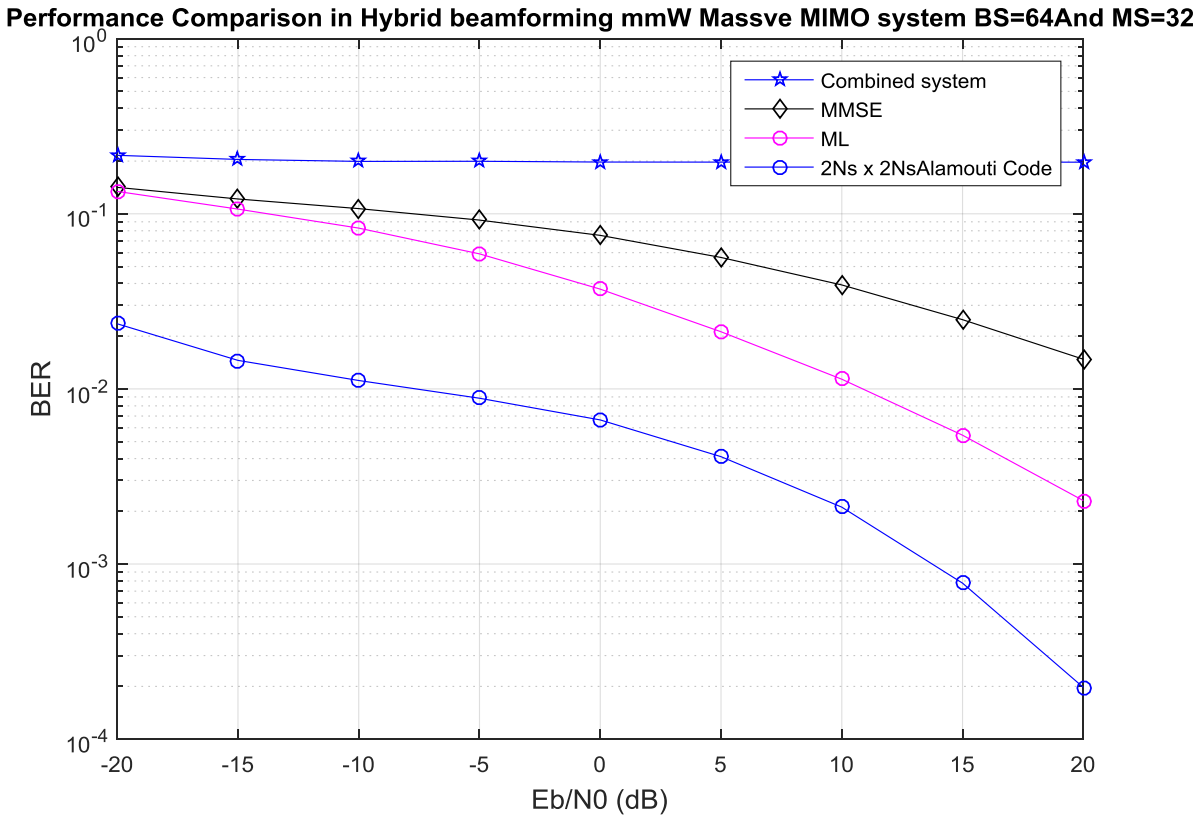


Figure 3.11. BER performance for uncoded single-cell hybrid beamforming mmW massive MIMO system on downlink transmission for $N_{BS} = 64$ and $N_{MS} = 32$ with 10 and 6 RF chains respectively, with $N_S = \mathrm{L} = 2$ for the MMSE, ML detectors, and combined system using BPSK modulation, and $N_S = \mathrm{L} = 2$ for the Alamouti code system using QPSK modulation at AOA/AOD resolution parameter $N = 162$ and beamforming vectors $K = 3$.

Now, let us consider that we have the same number of BS and MS antennas but with 3 RF chains at both sides. As can be seen from Figure 3.12, the Alamouti code still achieves the smallest BER values over the total range of $\frac{E_b}{N_0}$ , and the combined system also still has the highest ones. In addition, the ML detector performs better than the MMSE detector over the total range of $\frac{E_b}{N_0}$; a bit error probability of $10^{-2}$ can be obtained with $\frac{E_b}{N_0} = 16\,dB$ using the ML detector, whereas the MMSE detector needs more than $20\,dB$ which is significantly higher to

obtain the same BER. Moreover, as shown in Figure 3.12, the Alamouti code outperforms the other schemes including the combined system; at a bit error rate of $10^{-2}$, the performance of Alamouti code is still better than the ML, MMSE detectors, with performance improvements equal to $8\ dB$ and more than $12\ dB$ respectively.

By comparing the results from both Figures 3.11 and 3.12, it is observed that the performance of the 10 and 6 RF chains Alamouti code as shown in Figure 3.11 outperforms the performance of the 3 RF chains Alamouti as can be seen in Figure 3.12 with approximately $16\ dB$, and $3\ dB$ gains at a bit error probability of $10^{-2}$, and $10^{-3}$ respectively. Also, the performance of the 10 and 6 RF chains ML detector as shown in Figure 3.11 outperforms the performance of the 3 RF chains ML from Figure 3.12 with about $5\ dB$ gain at a bit error probability of $10^{-2}$. Moreover, a bit error probability of $10^{-1}$ can be obtained with $\frac{E_b}{N_0} = -8\ dB$ using the 10 and 6 RF chains MMSE detector as shown in Figure 3.11 while the 3 RF chains MMSE detector needs about $6\ dB$, with a $14\ dB$ gain to obtain the same BER.

The performance of all previous simulations can be improved by increasing the AOA/AOD resolution parameter $N$ and beamforming vectors $K$ resulting in the increase of the total number of adaptive stages; however, increasing the number of adaptive stages might cause higher training overhead for mmW channel estimation. However, in this thesis, we do not explore these facts.

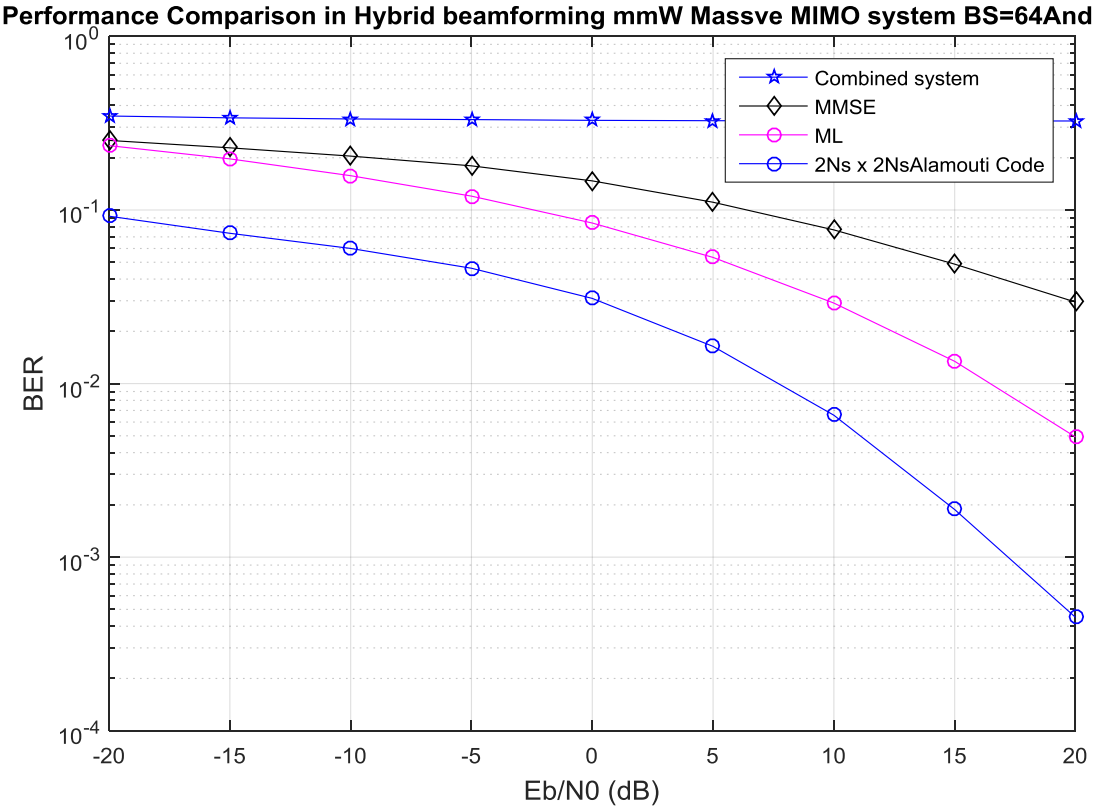


Figure 3.12 BER performance for uncoded single-cell hybrid beamforming mmW massive MIMO system on downlink transmission for $N_{BS} = 64$ and $N_{MS} = 32$ with 3 RF chains at both sides and $N_S = \mathrm{L} = 2$ for the MMSE, ML detectors, and combined system using BPSK modulation, and $N_S = \mathrm{L} = 2$ for the Alamouti code systems using QPSK modulation at AOA/AOD resolution parameter $N = 162$ and beamforming vectors $K = 3$.

In conclusion, it is clear that when we increase the number of RF chains, the performance of ML and MMSE detectors and Alamouti code is improved because of the improvement of the mmW channel estimation.

### 3.4.4 Performance Evaluation of ML and MMSE Detector and Alamouti Code with Perfect Channel State Information at Both MS and BS.

In this simulation, we evaluate the effect of different numbers of data streams on the performance of all schemes with perfect mmW channel state information at both BS and MS. In addition, the hybrid precoder uses a perfect mmW channel to precode the data streams to MS in the downlink transmission. We also use the hybrid combiner with a perfect mmW channel at MS to combine the received signal (combined system); then the ML, MMSE detectors and Alamouti code use perfect knowledge of the channel to detect the data streams.

Firstly, the BS has $N_{BS} = 64$ antennas, and the MS has $N_{MS} = 32$ antennas with a small number of RF chains; and then, we test the case of having a smaller number of MS antennas with the same number of RF chains $N_{RF}$ in order to test the antenna array gain performance at MS. Note that in these simulations we use the minimum number of RF chains for $N_S = 2, \text{and } 3$ in order to evaluate the performance of all schemes by assuming a number of multiplexed streams $N_s = L$ the number of mmW channel paths, where $N_s \leq N_{RF}$. Therefore, we used 3 RF chains for $N_S = 3$, and 2 RF chains for $N_S = 2$.

Figure 3.13 shows the BER performance results for downlink transmission by using QPSK modulation for $N_{BS} = 64$, $N_{MS} = 32$ with 3 RF chains at both sides. We compare the performance of MMSE, ML detectors and combined data streams system at the MS with $N_S = 3$. Figure 3.13 shows that the ML and MMSE detectors perform significantly better than the combined system over the higher range of $\frac{E_b}{N_0}$ (approximately from -10 to 10 dB); however all schemes have the same performance over the lower range of $\frac{E_b}{N_0}$ values (approximately from -40 to -11 dB). In addition, the performance of combined system is much better compared to the

previous sections because we assume a perfect mmW channel available at BS and MS. Moreover, the ML detector achieves the smallest BER values over the higher range of $\frac{E_b}{N_0}$ values; a bit error probability of $10^{-3}$ can be obtained with $\frac{E_b}{N_0} = 6\,dB$ using the ML detector; whereas the MMSE detector needs about $10\,dB$, with $4\,dB$ gain to obtain the same BER.

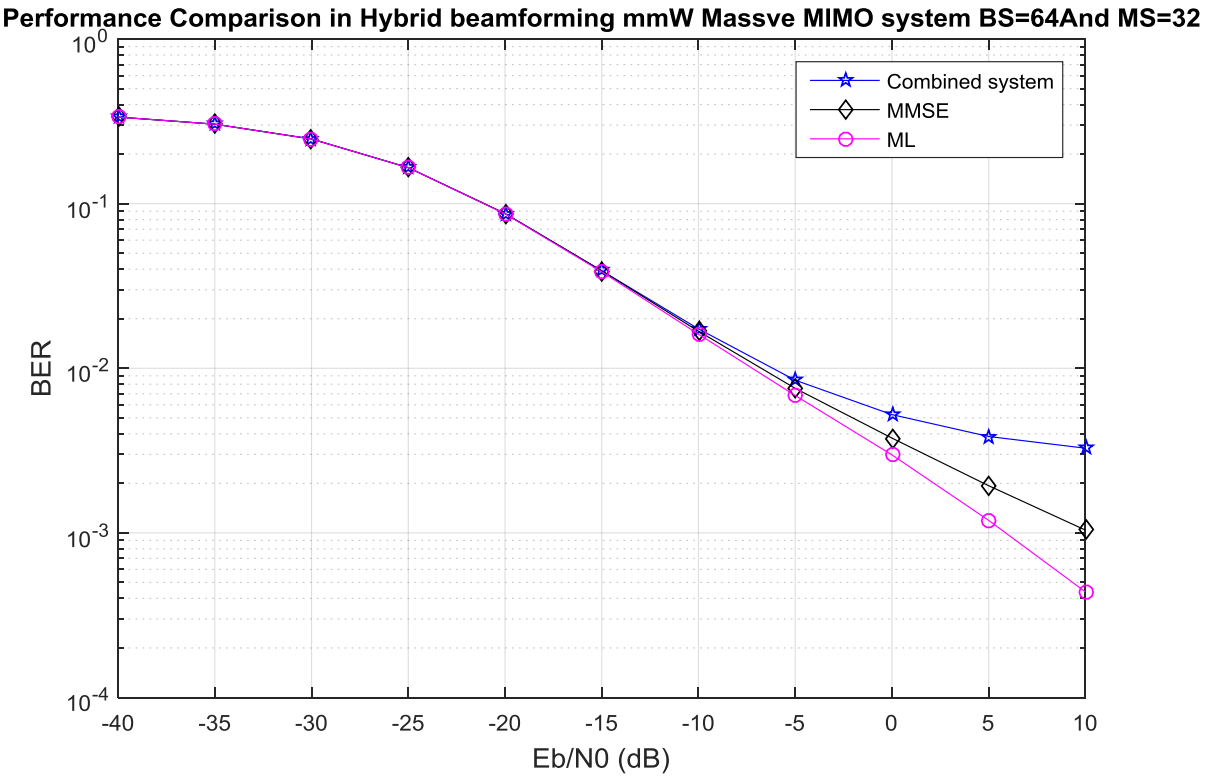


Figure 3.13. BER performance for uncoded QPSK single-cell hybrid beamforming mmW massive MIMO system on downlink with perfect CSI for $N_{BS} = 64$, $N_{MS} = 32$ with 3 RF chains at both sides and $\mathrm{L} = N_S = 3$.

In order to test the array gains performance of MS, we reduce the number of MS to 8 but keep the same number of RF chains and $N_S$ data streams. Figure 3.14 shows the BER performance results for downlink transmission by using QPSK modulation for $N_{BS} = 64$, $N_{MS} = 8$ with 3 RF chains at both sides. As can be seen from the plot, the total performance of all schemes is degraded compared to the results from Figure 3.13 due to the lower number of MS antennas

causing lower array gains. It also shows that the ML and MMSE detectors perform better than the combined system over the higher range of $\frac{E_b}{N_0}$ (approximately from -5 to 10 dB); however all schemes have the same performance over the lower range of $\frac{E_b}{N_0}$ values (approximately from -40 to -6 dB). Moreover, as shown in Figure 3.14, ML detector outperforms the other schemes over the higher range of $\frac{E_b}{N_0}$. In particular, at a bit error rate of $10^{-2}$, the performance improvements compared to the combined system and the MMSE detector are approximately 6 $dB$ and 2 $dB$ respectively.

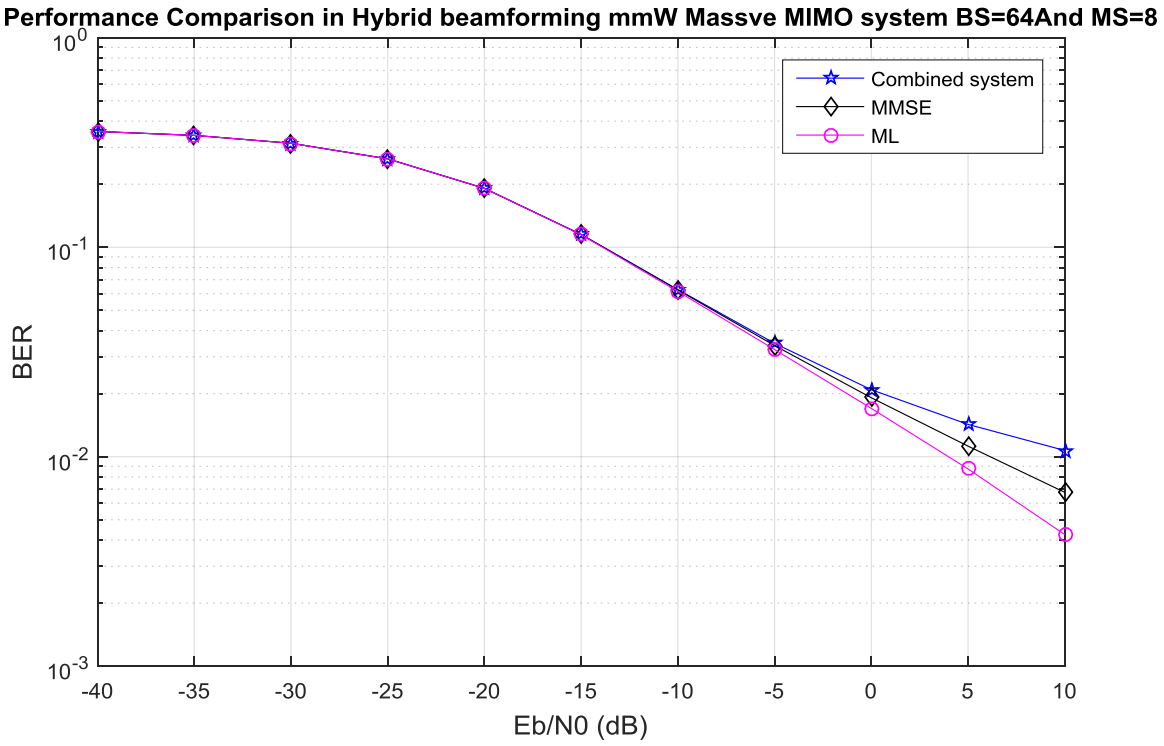


Figure 3.14 BER performance for uncoded QPSK single-cell hybrid beamforming mmW massive MIMO system on downlink with perfect CSI for $N_{BS} = 64$, $N_{MS} = 8$ with 3 RF chains at both sides, and L = $N_S = 3$.

By comparing the results from both figures 3.13 and 3.14, it is observed that the 64 x 32 with 3 RF chains and $N_S = \mathrm{L} = 3$ ML, MMSE detectors and combined system as shown in Figure 3.13 outperforms the 64 x 8 with 3 RF chains $N_S = \mathrm{L} = 3$ ML, MMSE and combined system as can be seen in Figure 3.14 with approximately 11 $dB$, 13 $dB$ and 16 $dB$ gains respectively at a bit error probability of $10^{-2}$.

Now we repeat the same process for $N_S = 2$. Figure 3.15 shows the BER performance results for downlink transmission by using QPSK modulation for $N_{BS} = 64$, $N_{MS} = 32$ with 2 RF chains at both sides, and $\mathrm{L} = N_S = 2$. As can be seen from the plot, the ML and MMSE detectors perform better than the combined system over the higher range of $\frac{E_b}{N_0}$ (approximately from -10 to 10 dB); however all schemes have the same performance over the lower range of $\frac{E_b}{N_0}$ values (approximately from -40 to -11 dB). Moreover, the ML detector achieves the smallest BER values over the higher range of $\frac{E_b}{N_0}$ values; at a bit error probability of $10^{-3}$, the ML detector outperforms the MMSE detector and combined system with 2 $dB$ and more than 10 $dB$ gains respectively.

Then, we reduce the number of MS antennas to 8 but keep the same number of RF chains and $N_S$ data streams. Figure 3.16 shows the BER performance results for downlink transmission by using QPSK modulation for $N_{BS} = 64$, $N_{MS} = 8$ with 2 RF chains at both sides. As can be seen from the plot, the total performance of all schemes is poor compared to the results from Figure 3.15 because of the lower array gains. Also, Figure 3.16 shows that the ML and MMSE detectors still perform better than the combined system over the higher range of $\frac{E_b}{N_0}$ (approximately from -5 to 10 dB); however all schemes have the same performance over the lower range of $\frac{E_b}{N_0}$ values (approximately from -40 to -6 dB). Moreover, as shown in Figure 3.16, the ML detector still

outperforms the other schemes; in particular, a bit error rate of $10^{-3}$ can be obtained with $\frac{E_b}{N_0} = 10\ dB$ using the ML detector; whereas the MMSE detector and combined system need more than $10\ dB$ to obtain the same BER.

By comparing the results from Figures 3.15 and 3.16, it is observed that the 64 x 32 with 2 RF chains and $N_S = \mathrm{L} = 2$ ML, MMSE detectors and combined system as shown in Figure 3.15 outperforms the 64 x 8 with 2 RF chains and $N_S = \mathrm{L} = 2$ ML, MMSE and combined system as can be seen in Figure 3.16 with approximately 9 $dB$, 9 $dB$ and 10 $dB$ gains respectively at a bit error probability of $10^{-2}$.

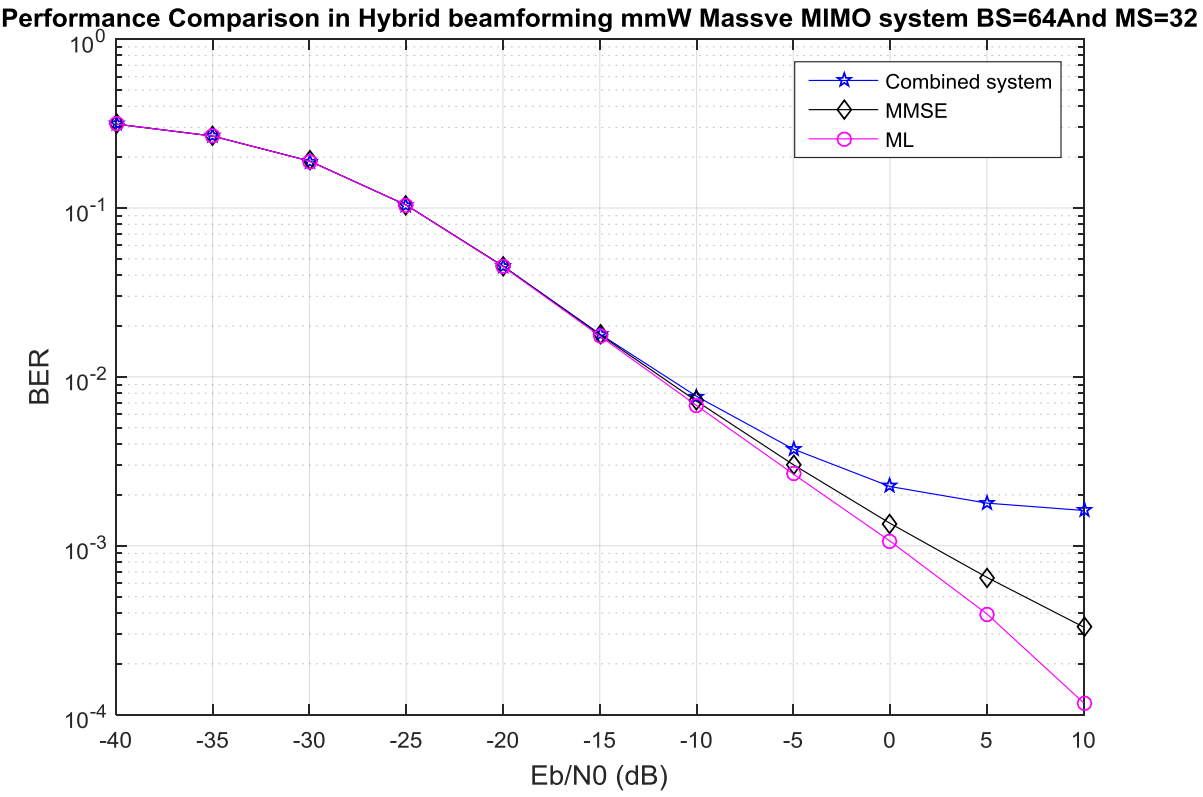


Figure 3.15. BER performance for uncoded QPSK single-cell hybrid beamforming mmW massive MIMO system on downlink with perfect CSI for $N_{BS} = 64$, $N_{MS} = 32$ with 2 RF chains at both sides, and $\mathrm{L} = N_S = 2$.

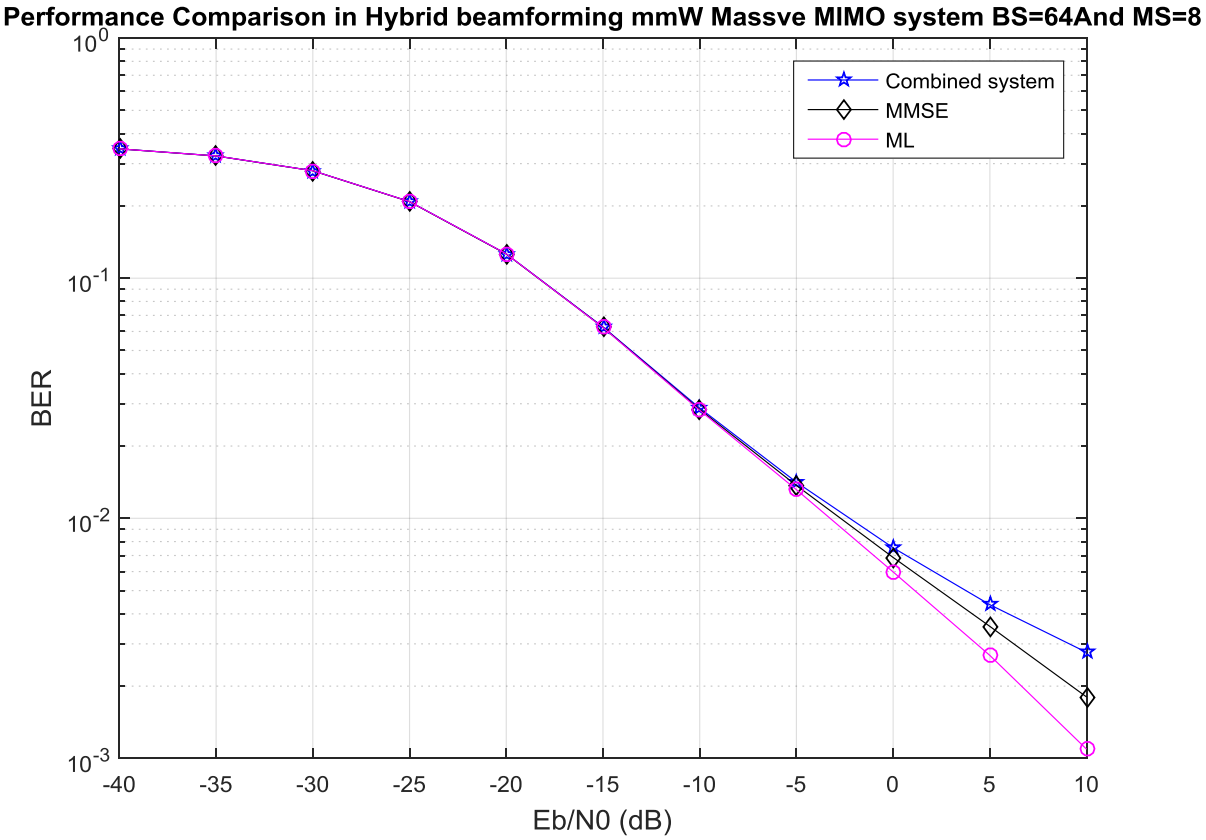


Figure 3.16. BER performance for uncoded QPSK single-cell hybrid beamforming mmW massive MIMO system on downlink with perfect CSI for $N_{BS} = 64$, $N_{MS} = 8$ with 2 RF chains at both sides, and L = $N_S = 2$.

Again, we repeat the same process for $N_S = 2$ but we compare the ML, MMSE detectors, and combined system with the Alamouti code. Figure 3.17 shows the BER performance results for downlink transmission for $N_{BS} = 64$ and $N_{MS} = 32$ with 2 RF chains at both sides. We use BPSK modulation with data streams $N_S = \mathrm{L} = 2$ for the MMSE, ML detectors, and combined system, and QPSK modulation with $N_S = \mathrm{L} = 2$ for Alamouti code system in order to make a fair comparison between all systems, where the MS in all systems receives the same number of bits per channel use. In addition, the mmW channel remains constant during the two time slots. As can be seen from the plot, the Alamouti code achieves the smallest BER values over the total

range of $\frac{E_b}{N_0}$ ; however, the ML detector performs better than the MMSE detector and combined system over all higher range of $\frac{E_b}{N_0}$ (approximately from -5 to 10 dB) and the MMSE performs similarity to the combined system over the total range of $\frac{E_b}{N_0}$. The performance of ML and MMSE detectors and combined system is the same over the lower range of $\frac{E_b}{N_0}$ values (approximately from -40 to -6 dB). Moreover, as shown in Figure 3.17, the ML detector outperforms the MMSE detector and combined system; in particular, a bit error rate of $10^{-3}$ can be obtained with $\frac{E_b}{N_0} = 1\,dB$ using the ML detector; whereas the MMSE detector and combined system need about $3\,dB$ to obtain the same BER.

Moreover, as shown in Figure 3.17, the Alamouti code outperforms the other schemes including the combined system. In particular, at a bit error rate of $10^{-3}$, the performance improvements compared to the ML and MMSE detectors and combined system are approximately $17\,dB$ ,$19\,dB$ and $19\,dB$ respectively. In addition, at a bit error rate of $10^{-4}$, the Alamouti code needs approximately $\frac{E_b}{N_0} = -10\,dB$ while the ML, MMSE detectors and combined system need more than $10\,dB$ to achieve this bit error rate.

Figure 3.18 shows the BER performance results for downlink transmission for $N_{BS} = 64$, $N_{MS} = 8$ with 2 RF chains and $N_S = 2$ at both sides for all sachems. As can be seen from the plot, the total performance of all schemes works poorly compared to the results from Figure 3.17 because of the lower array gains. The Alamouti code still outperforms the other schemes including the combined system. In particular, at a bit error rate of $10^{-2}$, the performance improvements compared to the ML is $13\,dB$, and $14\,dB$ compared to the MMSE detector and combined system which have the same performance over the total range of $\frac{E_b}{N_0}$ . Now, by

comparing the results from both Figures 3.17 and 3.18, it is observed that the 64 x 32 with 2 RF chains and $L = N_S = 2$ BPSK ML, MMSE detectors and combined system including the $L = N_S = 2$ QPSK Alamouti code as shown in Figure 3.17 outperform the 64 x 8 with 2 RF chains and $L = N_S = 2$ BPSK ML, MMSE and combined system including the $L = N_S = 2$ QPSK Alamouti code as can be seen in Figure 3.18 with approximately 9 $dB$, more than 7 $dB$, more than 7 $dB$, and 6 $dB$ gains respectively for all schemes at a bit error probability of $10^{-3}$.

In conclusion, when we decrease the number of MS antennas, the antenna array gain is decreased causing poor performance in all schemes.

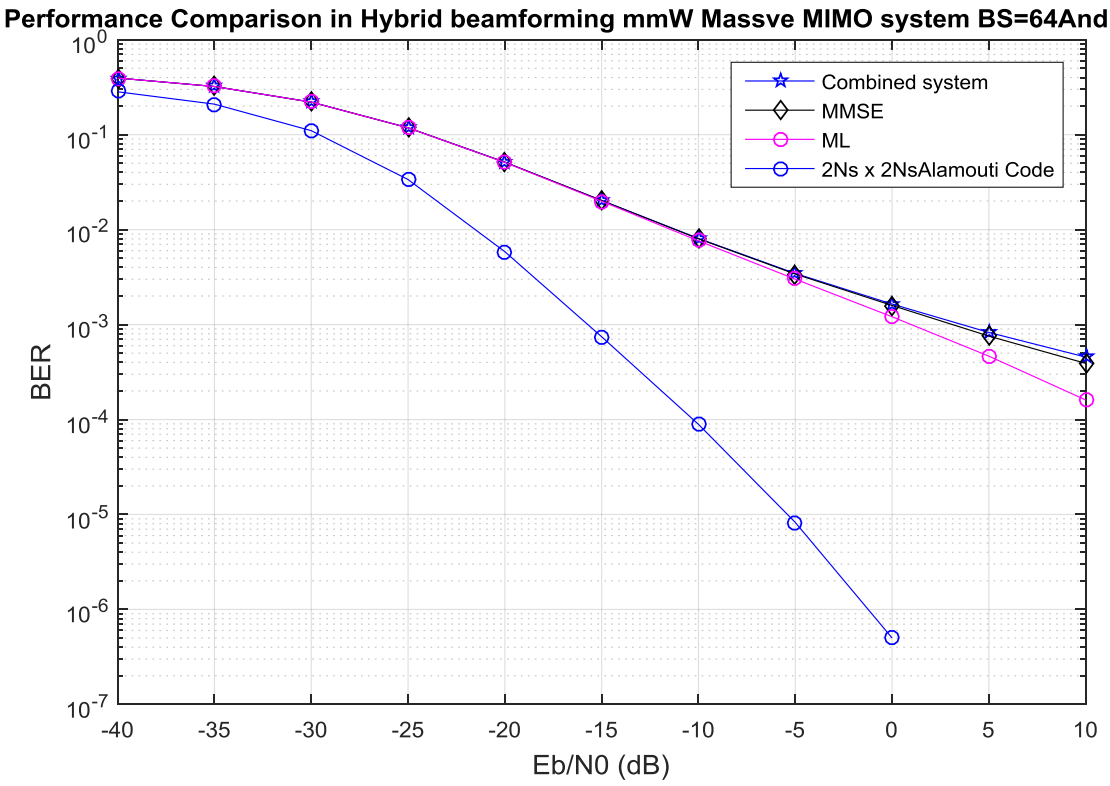


Figure 3.17. BER performance for uncoded single-cell hybrid beamforming mmW massive MIMO system on downlink transmission with perfect CSI for $N_{BS} = 64$ and $N_{MS} = 32$ with 2 RF chains at both sides and $L = N_S = 2$ for the MMSE, ML detectors, and combined system using BPSK modulation, and $L = N_S = 2$ for the Alamouti code systems using QPSK modulation.

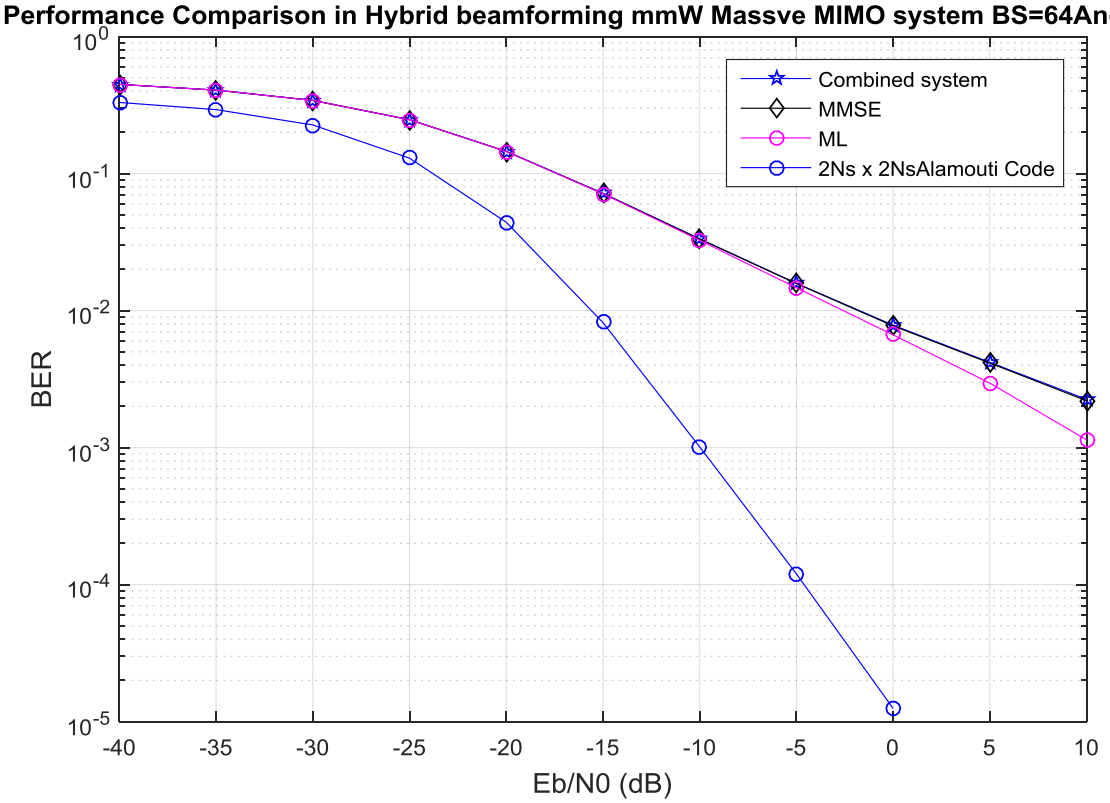


Figure 3.18. BER performance for uncoded single-cell hybrid beamforming mmW massive MIMO system on downlink transmission with perfect CSI for $N_{BS} = 64$ and $N_{MS} = 8$ with 2 RF chains at both sides and $L = N_S = 2$ for the MMSE, ML detectors, and combined system using BPSK modulation, and $L = N_S = 2$ for the Alamouti code systems using QPSK modulation.

Chapter 4

# Conclusion

## 4.1 Overview of Research

In this thesis, we examined the performance of Alamouti code implemented with a small number of transmit and receive antennas in classical MIMO systems. We observed that the 2x2 Alamouti system yielded the smallest BER values over the total range of $\frac{E_b}{N_0}$ compared to the 2x1 Alamouti system and because of this additional receiver, its diversity is increased. In addition, the SISO system has the highest BER values for all $\frac{E_b}{N_0}$ values because of no diversity. Then, we investigated massive MIMO system and evaluated the performance of uplink and downlink transmission in the lower frequency bands with different number of BS antennas, $N_t$ serving $K = 10$ users. Although the MRC/MRT requires the lowest complexity among the detectors and precoders such as ZF and MMSE, it performs poorly. However, the BER obtained by MRC/ MRT decreased and might be acceptable by significantly increasing the number of BS antennas $N_t$; therefore, it is better to use MRC/MRT due to its lower complexity compared to the ZF and MMSE detector/precoder when the number of antennas is high.

After that, we moved into mmW massive MIMO systems and showed that the schemes that are used by classical MIMO and massive MIMO can be exploited by hybrid beamforming mmW massive MIMO system. For example, the Alamouti code, ML and MMSE detectors can be used by hybrid beamforming mmW massive MIMO to improve the overall performance. Therefore, the aim of this study is to minimize the BER performance of hybrid beamforming mmW massive MIMO system applied on the downlink transmission through the use of the ML and MMSE

detectors and Alamouti code compared to an uncoded hybrid beamforming mmW massive MIMO system that uses hybrid combiner to combine the received data streams.

## 4.2 Summary of Results

This study examined some key aspects of implementing several schemes in the hybrid beamforming mmW massive MIMO systems and came up with the following conclusion:

- Concerning the downlink transmission on the hybrid beamforming mmW massive MIMO system using the channel estimation at the BS and perfect channel at MS, the ML, MMSE detectors and Alamouti code outperform the combined system over the entire range of $\frac{E_b}{N_0}$ for all simulations by considering all scenarios. In particular, when using $N_S = \mathrm{L} = 2$ or 3 data streams for downlink transmission using QPSK modulation, the ML detector achieves the smallest BER values over the higher range of $\frac{E_b}{N_0}$ but performs similarly to the MMSE detector over the lower range of $\frac{E_b}{N_0}$ with any number of RF chains. Moreover, when we use $N_S = \mathrm{L} = 2$ using BPSK modulation, the ML detector outperforms the MMSE detector over the higher range of $\frac{E_b}{N_0}$ (approximately from -20 to +20 dB) with any number of RF chains. When the Alamouti code uses $N_S = \mathrm{L} = 2$ using QPSK modulation and the ML and MMSE detectors use $N_S = \mathrm{L} = 2$ using BPSK modulation where the MS in all cases receives the same number of bits per channel use, the Alamouti code outperforms the ML and MMSE detectors in addition to the combined systems with any number of RF chains. Moreover, when we increase the number of RF chains, the performance of ML and MMSE detectors and Alamouti code

is improved because of the improvement of the mmW channel estimation compared to the cases with lower number of RF chains.

- When the downlink transmission of the hybrid beamforming mmW massive MIMO assumes a perfect mmW channel state information at BS and MS and uses the lowest RF chains at BS and MS, the $N_S = \mathrm{L} = 3$ or 2 ML and MMSE detectors using QPSK modulation perform significantly better than the $N_S = \mathrm{L} = 3$ or 2 combined system over the higher range of $\frac{E_b}{N_0}$ but all of them have the same performance over the lower range of $\frac{E_b}{N_0}$ values with the lowest RF chains and 32 or 8 MS antennas consideration. In addition, the $N_S = \mathrm{L} = 2$ Alamouti code using QPSK modulation performs significantly better compared to the $N_S = \mathrm{L} = 2$ ML, MMSE detectors and combined system using BPSK modulation in the case of using the lowest RF chains scenarios and 32 or 8 MS antennas where the MS in all systems receives the same number of bits per channel use. Moreover, it is clear that when the number of MS antennas is decreased from 32 antennas to 8 antennas using the lowest RF chains, the antenna array gain is degraded causing poor performance for all schemes.

## 4.3 Recommendation for Further Research

It has been shown that using the ML, MMSE detectors, and Alamouti code for hybrid beamforming mmW massive MIMO system on downlink transmission with a perfect or estimated CSI offers considerable improvement over the combined system. However, many questions remain unanswered after obtaining the results of the simulations done for this thesis.

Future research should apply these techniques to other mmW massive MIMO systems. First, wideband mmW systems are more likely to be operated over frequency-selective fading channels; therefore, we should investigate how the ML, MMSE detectors or another type of detection and the Alamouti code or another type of code perform in the wideband mmW systems. Second, simultaneous transmission to multiple users, which requires multi-user precoding at the transmitter, is also considered for mmW systems, so it will be interesting to apply these techniques and see their effects on the overall performance of mmW systems.

# References:


[1] T. L. Marzetta, “Noncooperative cellular wireless with unlimited numbers of base station antennas,”

IEEE Commun, vol. 9, no. 11, pp. 3590–3600, Nov. 2010.

[2] S.M.Alamouti, “A simple transmit diversity technique for wireless communications”, IEEE Journal, vol. 16, No. 8, October 1998

[3] H.Jafarkhani, “ Space-time coding”, Cambridge, 2005

[4] V.Tarokh, H.Jafarkhani, and A.R.Calderbank, “ Space-time block codes from orthogonal designs”, IEEE Trans. Inform. Theory, vol.45, No 5, July 1999.

[6] LuLu, G.Y.Li, L.Swindlehurst, A.Ashikhmin, and R.Zhang, “ An overview of massive mimo: benefits and challenges”, IEEE Journal In Signal Process, vol. 8, No 5, October 2014.

[7] T.Endeshaw and L.Bao Le, ” Massive MIMO and Millimeter Wave for 5G Wireless HetNet: Potentials and Challenges” , IEEE Vehicular Technology Magazine, arXiv:1510.06359v1 ,21 Oct 2015

[8] F.A.P.de Figueiredo, J. P. Miranda, ”Uplink Performance Evaluation of Massive MU-MIMO Systems”, Research and Development Center on Telecommunications, Brazil, arXiv:1503.02192v1 , 7 Mar 2015

[9] H.Q. Ngo, E.Larsson and T.Marzetta, “Energy and Spectral Efficiency of Very Large Multiuser MIMO Systems”, IEEE Transactions on Communications, vol. 61, NO. 4, APRIL 2013

[10] M.khalighi, K.Raoof and J.Genevieve, ”Capacity of Wireless Communication Systems Employing Antenna Arrays, a Tutorial Study”, Wireless Personal Communications 23: 321–352, 2002.

[11] Y.S.Cho, J .Kim, W.Y.Yang and C.G. Kang, “MIMO-OFDM WIRELESS COMMUNICATIONS WITH MATLAB”, 2010

[12] V.Mathuranathan, ”Characterizing a MIMO channel – Channel State Information (CSI) and Condition number”, August 20, 2014

[13] I.Poole, “MIMO Space Time Block Coding and Alamouti Codes”

[14] V .Tarokh, “ Space-Time Codes for High Data Rate Wireless Communication: Performance Criterion and Code Construction” , IEEE Trans. Inform. Theory, vol.44, No 2, March 1998.

[15] G.D.Golden, C.J.Foschini, R.A.Valenzuela and P.W.Wolniansky, “ Detection algorithm and initial laboratory results using V-BLAST space-time communication architecture” , IEEE Trans. Inform. Theory, vol.35, No 1, Jan 1999.

[16] E.G.Larsson, S.O.Edfors, F.Tufvesson, and B.Labs “Massive MIMO for next Generation Wireless Systems”, IEEE Communication Magazine Feburary 2014.

[17] K.Hosseini, J.Hoydis, S.Brink and M.Debbah “ Massive MIMO and Small Cells: How to Densify Heterogeneous Networks”, IEEE ICC 2013

[18] N.Q.Hien, “Fundamentals and System Designs”, Linköping Studies in Science and Technology Dissertations, No. 1642, Linköping University, 2015.

[19] T.S.Rappaport, S.Sun, R.Mayzus, H.Zhao, Y.Azar, K.Wang, G.Wong, J. K. Schulz, M. Samimi and F.Gutierrez, "Millimeter Wave Mobile Communications for 5G Cellular: It Will Work!" Nyu wireless, May 29, 2013

[20] J.G.Andrews, T.Bai, M.Kulkarni, A.Alkhateeb, "Modeling and Analyzing Millimeter Wave Cellular Systems", IEEE Transactions on Communications 13 May 2016

[21] O.El.Ayach, S.Rajagopal, S.Abu-Surra, Z .Pi, and R.W.Heath, " Spatially Sparse Precoding in Millimeter Wave MIMO Systems" , IEEE Transactions on Wireless Communications, VOL. 13, NO. 3, MARCH 2014

[22] A.Alkhateeb, O.El.Ayach , G.Leus , and R.W.Heath, "Channel Estimation and Hybrid Precoding for Millimeter Wave Cellular Systems" IEEE Journal of Selected Topics in Signal Processing, vol. 8, NO. 5, October 2014.

[23] G. R.M.Cartney, M.K. Samimi and T.S.Rappaport, " Exploiting Directionality for Millimeter-Wave Wireless System Improvement", Nyu Wireless, IEEE International Conference on Communications (ICC ), June 2015.

[24] Y.Niu, Y.Li, D.Jin, L.Su and A.V.Vasilakos, "A Survey of Millimeter Wave (mmWave) Communications for 5G: Opportunities and Challenges", arXiv:1502.07228v1 [cs.NI] 25 Feb 2015.

[25] R.W.Heath, N.Gonzalez-Prelcic, S.Rangan, W.Roh, and A.Sayeed" An Overview of Signal Processing Techniques for Millimeter Wave MIMO Systems", IEEE Journal of Selected Topics in Signal Processing, vol. 10, no. 3, April 2016.

[26] J.Lee, J.Liang, H.K.Kwon, and M.D.Kim, "Site-Specific Path Loss Characteristics with Directional Antenna Measurements at 28 GHz in Urban Street Grid Environments", Electronics and Telecommunications Research Institute (ETRI), IEEE 2015 26th.

[27] S.Sun, T.S.Rappaport, S.Rangan, T. A.Thomas, A .Ghosh, I .Z. Kov, I .Rodriguez, O .Koymen and A.Partyka, "Propagation Path Loss Models for 5G Urban Micro and Macro-Cellular Scenarios" New York University, Brooklyn, NY, USA, IEEE, 2016

[28] G.R.M.Cartney and M. K.Samimi, " Omnidirectional Path Loss Models in New York City at 28 GHz and 73 GHz", Nyu Wireless, Sept 2 - 5, 2014.

[29] S.Sun and G.R.M.Cartney, "Millimeter-Wave Distance-Dependent Large-Scale Propagation Measurements and Path Loss Models for Outdoor and Indoor 5G Systems", New York University, Brooklyn, NY, USA 11201, April. 2016.

[30] M.K.Samimi and T.S.Rappaport, "Statistical Channel Model with Multi-Frequency and Arbitrary Antenna Beamwidth for Millimeter-Wave Outdoor Communications," in 2015 IEEE Global Communications Conference, Exhibition & Industry Forum (GLOBECOM) Workshop, Dec. 6-10, 2015.

[31] X.Gao, L.Dai, S.Han, C.Lin and R. W. Heath, " Energy-Efficient Hybrid Analog and Digital Precoding for MmWave MIMO Systems With Large Antenna Arrays", IEEE Journal on Selected Areas in Communications, vol. 34, NO. 4, APRIL 2016

[32] S.Gimenez , S .Roger , P.Baracca , D.Martín-Sacristán, J. F. Monserrat , V .Braun and H .Halbauer, "Performance Evaluation of Analog Beamforming with Hardware Impairments for mmW Massive MIMO Communication in an Urban Scenario", Article, 22 September 2016.

[33] S.Mumtaz, J.Rodregues, and L.Dia, " mmWave Massive MIMO A Paradigm For 5G", book, India,2016.

[34] R.M.Rial , C .Rusu , A .Alkhateeb , N.G.Prelcic , and R.W. Heath, "Channel Estimation and Hybrid Combining for mmWave: Phase Shifters or Switches?", The University of Texas at Austin

[35 J.Mo, A.Alkhateeb, S .A Surra and R.W. Heath, " Achievable Rates of Hybrid Architectures with Few-Bit ADC Receivers", The University of Texas at Austin, March 9-11, 2016.

[36] T.Xie, L.Dai, X .Gao, M .Z Shakir, and Z .Wang, " GMD-Based Hybrid Precoding For Millimeter-Wave Massive MIMO Systems", arXiv:1605.04686v1, 16 May 2016

[37] H.L.V.Trees, "Optimum array processing (detection, estimation, and modulation theory, Part IV)," Wiley-Interscience, Mar, no. 50, p. 100, 2002.

[38] H.Zhu, G. Leus, and G. Giannakis, "Sparse regularized total least squares for sensing applications," in Proc. IEEE 11th Int. Workshop Signal Process. Adv. Wireless Commun. (SPAWC), Marrakech, Morocco,Jul. 2010, pp. 1–5.

[39] C.Ekanadham, D.Tranchina, and E.P.Simoncelli, "Recovery of sparse translation-invariant signals with continuous basis pursuit," IEEE Trans. Signal Process., vol. 59, no. 10, pp. 4735–4744, Oct.2011.

[40] D.Ramasamy, S.Venkateswaran, and U. Madhow, "Compressive parameter estimation in AWGN," ArXiv, 2013 arXiv:1304.7539.

[41] M.Rossi, A.Haimovich, and Y.Eldar, "Spatial compressive sensing for MIMO radar," IEEE Trans. Signal Process., vol. 62, no. 2, pp. 419–430, Feb. 2014.

[42] M.L.Malloy and R.D.Nowak, "Near-optimal compressive binary search," ArXiv, 2012 arXiv:1306.6239.

[43] M.Iwen and A.Tewfik, "Adaptive strategies for target detection and localization in noisy environments," IEEE Trans. Signal Process., vol. 60, no. 5, pp. 2344–2353, May 2012.

[44] N.Srivastsva, "DIVERSITY SCHEMES FOR WIRELESS COMMUNICATIONA SHORT REVIEW", Department of Electronics, Institute of Engineering & Technology, Lucknow Uttar Pradesh, India-226021, 31st May 2010. Vol.15. No.2.

[45] G.J. Foschini and M.J.Gans, "On limits of wireless communication in a fading environment when using multiple antennas," Wireless Personal Commun., Mar. 1998.

[46] A. Alkhateeb, G. Leus, and R. W. Heath, "Limited feedback hybrid precoding for multi-user millimeter wave systems," IEEE Trans. Wireless Commun., vol. 14, no. 11, pp. 6404–6481, Nov. 2015.